

**TRENDS IN THE WAVINESS OF THE SOUTHERN HEMISPHERE SUBTROPICAL  
AND POLAR JETS**

by

**Taylor P. Norton**

A THESIS SUBMITTED IN PARTIAL FULFILLMENT OF THE REQUIREMENTS FOR  
THE DEGREE OF

Master of Science

(Atmospheric and Oceanic Sciences)

At the

**UNIVERSITY OF WISCONSIN-MADISON**

2024

## i. Abstract

Changes in jet stream behaviors have been found because of our warming world, though the waviness of jets has not been widely investigated in the Southern Hemisphere. Hence, the Southern Hemisphere wintertime polar and subtropical jets' evolution, especially with respect to their waviness, within the past century is examined in this thesis. The recently developed average latitudinal displacement (ALD) methodology is applied to assess the waviness of the austral-winter subtropical and polar jets using three different reanalysis data sets. As in the wintertime Northern Hemisphere (NH), both jets in the Southern Hemisphere have become systematically wavier over the time series (1958-2019) and the waviness of each jet evolves independently of the other during most cold seasons. Also, like its Northern Hemisphere equivalent, the Southern Hemisphere polar jet exhibits no trend in speed (though it is notably slower on average than the NH), while its poleward shift is statistically significant. In contrast to its Northern Hemisphere counterpart, the austral subtropical jet has undergone both a systematic increase in speed and a statistically significant poleward migration. Composite differences between the waviest and least wavy seasons for each jet species suggests that the Southern Hemisphere's lower-stratospheric polar vortex is negatively impacted by anomalously wavy tropopause-level jets of either species. These results are considered in the context of trends in the Southern Annular Mode as well as the findings of other related studies.

## ii. Acknowledgements

I would like to thank Jonathan Martin, my advisor, for his guidance and help in teaching me throughout my time as his student. I have learned to take new perspectives on problems and ask for help when needed. Jonathan's patience was highly appreciated as I worked through this period of my life. We were lucky enough to get a publication out of this work before I finished my entire thesis as well.

Another thank you to Matthew Lazzara for accepting me as his Project Assistant (PA) for the Antarctic Meteorological Research and Data Center (AMRDC). Also, Matthew's encouragement, advice, and input on my thesis and graduate work was much appreciated. His check ins helped aid my motivation in the writing process. As a mentor, Matthew truly was a light in my completion of my master's degree.

Linda Keller was a considerable help in analyzing the data I had and connecting the dots between what we were seeing and other possible relationships in the atmosphere. I'd like to thank her for her help and suggestions for my thesis. I'd also like to thank Dave Mikolajczyk, Lee Welhouse and Angie Montgomery for their support and bolstering of me finishing my degree.

I would like to thank my committee members, Angela Rowe and Hannah Zanowski, for their insightful comments and suggestions on my thesis. Their quick responses and aid in a busy time was very appreciated.

One of the largest thank yous goes to my husband, Logan Ziegler, who has been there for me every step of the way and supporting me when I needed it. I would also like to acknowledge his direct help in writing some of the code used to collect and organize data into properly formatted files. Getting through graduate school would have been impossible without him.

A monumental thank you to my family (my dad, Curt, my mom, Dawn, and my sister, Megan) and friends for their support and belief in my capability to really do this. Although these past few years have been some of the toughest, they have all made it so much brighter just being themselves and boosting my confidence.

I would also like to thank the U.S. National Science Foundation for the opportunity to receive my degree with support on grant numbers 1951720, 1924730, and 2301362 through AMRDC and the Automatic Weather Station project.

**iii. Table of Contents**

<b>1. Introduction .....</b>	<b>1</b>
<b>1.1 Southern Hemisphere Jet Climatologies .....</b>	<b>2</b>
<b>1.2 Climate Modes .....</b>	<b>6</b>
<b>2. Data and Methods .....</b>	<b>10</b>
<b>3. Results.....</b>	<b>22</b>
<b>3.1 Jet Waviness .....</b>	<b>22</b>
<b>3.2 Jet Strength .....</b>	<b>26</b>
<b>3.3 Jet Equivalent Latitude .....</b>	<b>30</b>
<b>3.4 Comparing ALD with SAM.....</b>	<b>32</b>
<b>3.5 Differences in Wavy Seasons .....</b>	<b>35</b>
<b>4. Discussion .....</b>	<b>38</b>
<b>4. 1 Connections to Climate Modes .....</b>	<b>39</b>
<b>5. Conclusions.....</b>	<b>40</b>
<b>6. References.....</b>	<b>41</b>

## 1. Introduction

The weather and climate of different regions are heavily influenced by the jet streams. Jet streams are meandering bands of strong winds in the atmosphere near the tropopause. The jet stream was first discovered by Wasaburo Ooishi (the first director of Japan's upper air observatory) in the early 1920s by launching a balloon with a theodolite at Tateno (Lewis 2003). Now it is known that two prominent jets exist in each hemisphere during the winter season: the subtropical (STJ) and polar (POLJ) jets. These jets flow from west to east but are undulatory north to south. Jet streams are also boundaries between warm and cold air and as one moves equatorward (particularly the POLJ), cold air is brought in from the poleward side and as a jet moves poleward, warm air follows from the equatorward side. The POLJ forms via eddy momentum flux convergence related to the development of midlatitude baroclinic waves (Martin 2021). The STJ forms from the angular momentum transport via the thermally direct Hadley circulation (Martin 2021). Due to the formation of these jets, the warming temperatures in the atmosphere from climate change are anticipated to have an impact on the jets' behavior.

Climate change has brought enhanced warming temperatures to the northern high latitudes, known as Arctic amplification (Francis and Vavrus 2012). Francis and Vavrus (2012) first suggested that the undulatory behavior of the jet stream could be linked to this amplification. They hypothesize two effects on upper-level environmental characteristics: 1) The strength of poleward thickness gradients affects upper-level zonal wind speeds - the weaker the gradient, the slower the winds and vice versa; 2) Arctic amplification causes 500 hPa heights to rise in the mid-latitudes which increases the wave amplitude of the polar jet and brings the peaks of the ridges poleward. Another factor found with slower zonal winds and higher wave amplitudes is a slower progression

of Rossby waves. The wave speed of a Rossby wave is  $c = \bar{u} - \frac{\beta}{K^2}$  where  $\bar{u}$  is the mean westerly flow,  $\beta$  is the Rossby parameter and  $K^2 = k^2 + l^2$  which is the total wavenumber squared (Holton 1992). Therefore, a wavier jet would decrease the wavenumber, leading to a slower progression of Rossby waves. It is this slowed progression that can cause more persistent weather conditions which can lead to extreme weather in the midlatitudes (Francis and Vavrus, 2012). Weaker zonal-mean, upper-level winds are associated with increased atmospheric blocking and cold outbreaks in the NH (Barriopedro and Garcia-Herrera, 2006; Vavrus et al. 2006).

The land-sea differences in each hemisphere change the jet's general behavior. The northern hemisphere (NH) has much more land in the midlatitudes compared to the southern hemisphere (SH) and the NH polar jet is more variable than its counterpart (Pena-Ortiz et al., 2013). This is because Antarctica's land mass sits over the polar cap where the air stays cold all year, creating a strong temperature gradient from the equator to the pole (Dätwyler et al. 2017). Around 60°S the Earth's surface is completely land free and allows less restricted airflow surrounding the continent as well (Dätwyler et al. 2017). Due to the warming temperatures, though, the temperature gradient will likely weaken and therefore may weaken the jets' strength.

## 1.1 Southern Hemisphere Jet Climatologies

Chenoli et al. (2017) gives an overview of the background of the SH STJ and POLJ. These jets influence many factors including storm tracks, surface cyclogenesis, and precipitation. Changes in the location, altitude and intensity can have major effects on the climate as well. Since there is limited land in the SH compared to the NH (Figure 1.1), the jets are much more zonally symmetric, but have large seasonal variability because of the strong temperature difference from the pole to the equator. The STJ has the strongest winds in the austral winter, particularly over

Australia and the western south Pacific Ocean, and is generally centered around the 30°S (Figure 1.1). The POLJ has the strongest winds from austral autumn to spring over the Atlantic and Indian Oceans. The Hadley Circulation (HC) and the STJ are closely tied, and the jet usually sits on the poleward edge of the HC boundary. As the HC expands and contracts, the STJ moves with it. Increased concentrations of greenhouse gases have expanded the HC and therefore, moved the STJ poleward. Chenoli et al. (2017) found that five climate models (GFDL-CM3, HadGEM2-ES, CanESM2, GISS-E2-R and CSIRO-MK3.6.0) showed a significant positive trend in the jet strength in the wintertime.

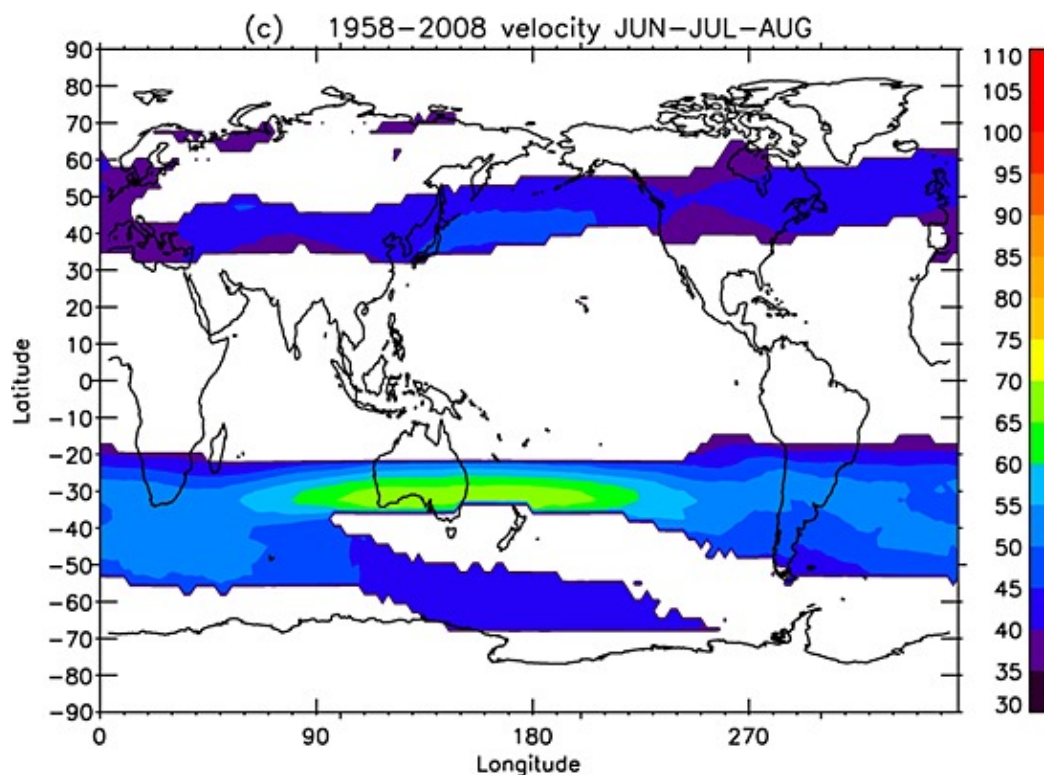


**Figure 1.1** From Chenoli et al. (2017), the averaged velocity of jet cores computed from the NCEP/NCAR Reanalysis over the period 1958–2008 for (c) JJA in  $\text{ms}^{-1}$ . The average velocity is depicted where the frequency of jet cores is higher than 1.5 days/month at each grid point.

Gillett et al. (2021) assesses the interannual variability of the STJ and found that two jets are clearly distinct in latitude during the austral winter where the mean position of the STJ is around  $27^{\circ}\text{S}$ . The mean strength of the STJ was found to be  $37.06 \text{ m s}^{-1}$ . The STJ was found to have a higher velocity in the winter versus the summer, averaging around  $45\text{-}50 \text{ m s}^{-1}$  and  $35 \text{ m s}^{-1}$ , respectively (Gallego et al. 2005). A stronger STJ is indicated to be found closer to the equator due to the high correlation between the intensity and position of the jet, agreeing with previous studies. The standard deviation (s.d.) of the magnitude of maximum westerly wind speed is  $1.85 \text{ m s}^{-1}$  and the s.d. of the latitude at which that speed is found is  $0.59^{\circ}$ .

Pena-Ortiz et al. (2013) proposed a different method to find the jet cores in the SH and NH jets. They computed the horizontal wind speed at each grid point to locate the local wind maximum at each longitude from 400-100 hPa. Using a threshold of  $30 \text{ m s}^{-1}$ , the frequency with which the local maxima was above the threshold for the days per month at each grid point is the probability of jet cores to occur at those locations. National Centers for Environmental Prediction (NCEP) reanalysis (Kalnay et al. 1996) and 20<sup>th</sup> Century Reanalysis V2 (20CR) (Compo et al. 2011) were the two datasets used in their study. They found the SH jets to be more zonally symmetric than in the NH and had distinct differentiation between the subtropical and polar jets. The maximum occurrence of jet cores was around  $25^{\circ}\text{S}$  showing that the STJ is likely more persistent across longitudes compared to the POLJ as there were areas of weakened jet core strength south of  $40^{\circ}\text{S}$ . The STJ had winds from  $40\text{-}65 \text{ m s}^{-1}$  and was found to be more stable than the POLJ as it seems to move poleward in austral winter while also being slightly slower with a range in speed from  $40\text{-}55 \text{ m s}^{-1}$ . These results were similar but stronger in shift strength than compared to Archer and Caldeira (2008). Although the STJ exhibits less variance in its latitude than the POLJ, the STJ has moved poleward in the SH winter months by  $0.3^{\circ} \text{ decade}^{-1}$  and  $0.1^{\circ} \text{ decade}^{-1}$  (NCEP and 20CR,

respectively). It was also found that the velocity of the POLJ increased minimally:  $\sim 0.3 \text{ m s}^{-1}\text{decade}^{-1}$ , though the two reanalyses showed varying results per time period (1958-2008 vs 1979-2008). The STJ has a statistically significant increase in velocity at  $0.6 \text{ m s}^{-1}\text{decade}^{-1}$ . All of these studies have covered the jets' position and strength but have not considered the waviness of the jets.

To my knowledge, Gallego et al. (2005) was the first to calculate an indicator for waviness. The algorithm to find both of the SH jets was by identifying 200-hPa geostrophic streamlines of maximum average velocity in the SH. The maximum velocity of these streamlines showed two maxima seasonally and therefore the locations of two jets. Computing the difference between the maximum and minimum latitude found each day for both jets gives the zonal index. Their study shows that from 1958-2002, the STJ increased in the zonal index, indicating the jet got wavier. The POLJ showed no significant trend in the zonal index over that time period. The STJ seems to have had a displacement change from 1958-1978 compared to 1979-2002 where the jet trends southward. The velocity of the STJ significantly decreases from 1958-1978 but the trend flattens from 1979-2002, nearly increasing. The POLJ had a significant decrease in latitude but an increase in velocity from 1958-2002. A similar metric, termed DayMaxMin, was employed by Barnes (2013) in her consideration of the behavior of the NH 500 hPa flow. Though insightful, such a metric does not comprehensively account for the waviness created by the full collection of troughs and ridges around the hemisphere that routinely characterizes the jets.

From all of these studies, there is consistent agreement on the poleward shift of both the STJ and POLJ in recent decades as well as a strengthening of the STJ and minimally of the POLJ. The location of the STJ varied slightly depending on the method used to identify the jets between previous studies, but all were between 25-30°S. The waviness of the STJ was noted to be

increasing while the POLJ had no significant trend. How the jets' trends compare to different climate modes may lead to more understanding of the jets' behaviors.

## 1.2 Climate Modes

The southern annular mode (SAM) has the most impact on atmospheric variability poleward of 20°S (Gallego et al. 2005) and is related to the oscillating of geopotential heights between the mid and high latitudes. As an internal mode of climate variability, SAM is naturally occurring, but can be impacted by external forcings including increased greenhouse gases and ozone depletion over the Antarctic (Fogt and Marshall 2020).

Gallego et al (2005) found that both the POLJ and STJ are influenced by SAM, with a more substantial impact imposed upon the POLJ. During the winter months, a positive phase in SAM tends to shift the POLJ poleward and increase the velocity up to 50% over the Pacific Ocean. The STJ shows a slower average velocity in the positive phase and moderate latitudinal changes, but there was a slight equatorward shift seen. In a negative phase of SAM, the STJ is stronger with higher velocities (up to 20%) over the Indian Ocean and West Pacific.

In the decades prior to 2000, the SH jets shifted poleward and the SAM has tended toward positive polarity (e.g., Fogt and Marshall, 2020). These coincident trends have been presumed to be a result of ozone depletion. As the ozone recovers in the SH, simulations suggest the jets' poleward shift and positive SAM polarity trend may reverse (WMO, 2022). Spensberger et al. (2020) have questioned whether the associated jet displacement also explains shifts in the storm tracks across the hemisphere. Instead they suggest that the SAM can be interpreted as a measure of the degree of coupling (or decoupling) between Antarctica and the southern mid-latitudes.

El Niño Southern Oscillation (ENSO) is a climate pattern that oscillates between cool and warm phases of the surface temperature across the equatorial Pacific Ocean. These phases also

shift wind and precipitation patterns in the tropics, which in turn leads to changes around the world. Gallego et al. (2005) studied the effects of the ENSO phases on the SH jets. They found that ENSO had more of an effect on the STJ than the POLJ, though overall the effect was smaller in strength and limited to smaller regions compared to SAM. Both jet positions had the largest difference in the Pacific sector (Figure 1.2) with the STJ having a greater difference from June to November. During an El Niño phase the STJ generally shifts equatorward in the Pacific sector while the POLJ shifts poleward in the same area. This is generally the opposite effect compared to SAM for the POLJ, but a similar displacement. The STJ shifts minimally between a negative and positive SAM, less so than between ENSO indices. Jet strength of the STJ was the most significant ENSO effect where the speed of the jet was 25-50% larger for El Niño versus La Niña over the Pacific. POLJ had an opposite effect where it decreased in speed during El Niño by 10-25%. In the Indian and Atlantic sectors, all of these changes are weaker and of opposite behavior (Figure 1.2). A stronger STJ is also highly correlated to El Niño and appears to stem from divergent outflow from the diabatic heating associated with El Niño (Gillett et al. 2021).

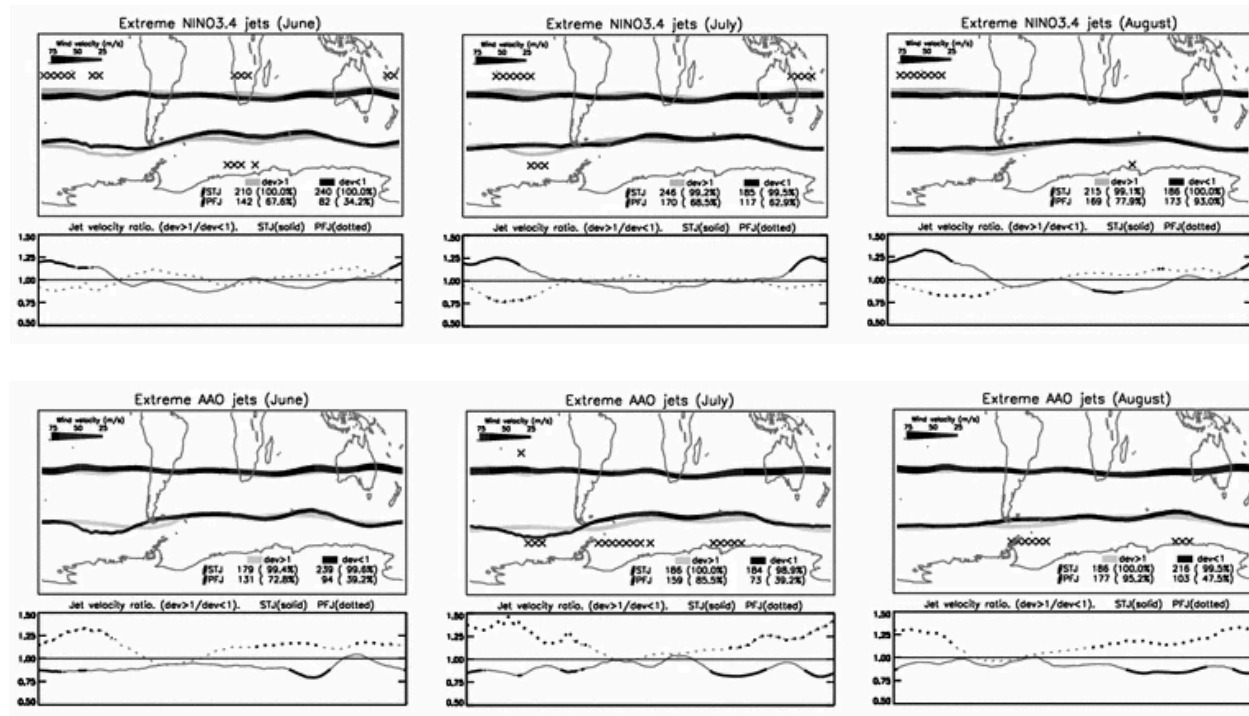


**Figure 1.2** From Gallego et al. 2005, the average jet path during extreme El Nino N3.4 indices and Antarctic Oscillation (AAO)/SAM phases for June, July and August. Black jets are negative phases/indices and gray are positive. X's indicate significant latitude differences between phases. Graphic below each figure shows the ratio between the jet velocity during positive/negative phases for the STJ (solid) and POLJ (dotted).

The SH circulation is strongly associated with two zonal wave numbers: 1 and 3 (Raphael 2004). Zonal wave 1 (ZW1) is zonally symmetric and the dominant wave for the climatological mean at 90% of the spatial variance at 60°S (Raphael 2004). Zonal wave 3 (ZW3) accounts for 8% of the spatial variance with maximum amplitudes around 50°S, though is still seen in daily, seasonal and interannual timescales. Raphael (2004) calculated the ZW3 index from 500hPa geopotential heights to study the negative and positive phases of ZW3. The positive phase indicates stronger and more meridional flow while the negative phase is weaker ZW3 and more zonal flow.

The zonal anomaly had differing variability in amplitude, though the variability strengthened in the 1980s. It was also found that from ~1960-1980 the negative phase was more dominant, but that trend shifted into the positive phase being more dominant into the 1990s. Raphael noted that ZW3 has an annual cycle as well and tends to be positive from midsummer to late winter with the strongest positive ZW3 occurring in winter. With an increasing trend in a positive ZW3, the waviness of the SH circulation may relate to the jets' waviness trends. The strongest negative ZW3 occurs in the spring. The amplitude of the zonal anomaly tends to be smaller more frequently compared to larger amplitudes.

Due to their possible links to storm track variability, climate modes, and other changes in weather patterns, the waviness and trends of the waviness of both the STJ and POLJ need to be assessed and understood. To accomplish this goal, the following study explores the austral wintertime waviness of the SH subtropical and polar jets as well as the climatologies of the jets' behaviors, including their average latitude at which they reside and the average speeds. These findings are also compared to those from the NH presented in a previous study by Martin (2021) and more generally with previous studies. The land-sea differences have a large effect on the two hemisphere's jet behaviors, but with a warming world, the waviness of the SH jets may have similar trends to the NH increasing waviness (Martin, 2021) if the temperature gradient weakens the flow of the jets. The methodology of finding the jets and calculating the waviness is described in Section 2. In section 3, the results of the jets' waviness and climatologies are interpreted. Section 4 compares results to previous studies and discusses possible explanations of the results. Finally, the conclusion of this paper is found in section 5.

## 2. Data and Methods

This study follows the procedure of Martin (2021), as previously applied to the NH, to find the waviness of the SH subtropical and polar jet streams. The jets are identified in potential temperature ( $\theta$ )/potential vorticity (PV) space following the objective method from Christenson et al (2017) for the Northern Hemisphere. A similar approach was taken by Maher et al. 2020 for the STJ. Specifically, jet cores are identified on the equatorward side of a strong PV gradient in certain isentropic layers (315:330K for POLJ and 340:355K for STJ). The quasi-geostrophic potential vorticity (QGPV) can be used to justify this PV gradient/jet relationship, and the equation is given by:

$$(1) q_g = \frac{1}{f_o} \nabla^2 \varphi + f + \frac{\partial}{\partial p} \left( \frac{f_o}{\sigma} \frac{\partial \varphi}{\partial p} \right) = \Lambda(\varphi) + f$$

(where  $\Lambda = \frac{1}{f_o} \nabla^2 + \frac{\partial}{\partial p} \left( \frac{f_o}{\sigma} \right) \frac{\partial}{\partial p} + \frac{f_o}{\sigma} \frac{\partial^2}{\partial p^2}$ ,  $p$  is pressure,  $f$  is the Coriolis parameter, and  $\varphi$  is the geopotential). The cross-jet gradient of QGPV ( $\frac{\partial q_g}{\partial n}$ , where  $\hat{n}$  is the cross directional flow in natural coordinates) can be shown as:

$$(2) \frac{\partial q_g}{\partial n} = \Lambda \left( \frac{\partial \varphi}{\partial n} \right) = \Lambda(-fV_g)$$

after substituting from the natural coordinate expression for geostrophic wind (Martin 2021). Hence, maxima in the cross-flow gradient of QGPV are collocated with maxima in the geostrophic wind.

The zonal ( $u$ ) and meridional ( $v$ ) winds as well as the temperature ( $T$ ) at 6 h intervals from three different reanalysis datasets were utilized in this study: Japanese 55-year (JRA-55), National Centers for Environmental Prediction/National Center for Atmospheric Research (NCEP/NCAR),

and European Centre for Medium-Range Weather Forecasts (ECMWF) Reanalysis v5 (ERA5). A total of 62 austral winters (June, July, August - JJA) from 1958-2019 of the JRA-55 were employed using data on 60 vertical levels up to 0.1 hPa on a horizontal grid mesh of ~55 km (Kobayashi et al. 2015). JJA data from NCEP/NCAR reanalysis at 17 isobaric levels to 10 hPa on a 2.5° latitude-longitude grid (Kalnay et al. 1996) from 1948-2019 was used. Finally, the ERA5 data on 137 vertical levels from the surface to 80 km with a grid spacing of 31 km covering the time period of 1979-2019 (Copernicus Climate Change Service [CS3], 2017) was also used. The different reanalyses have varying assimilation schemes and input data sets with some characterized by known discontinuities arising from the introduction of satellite data (e.g., Santer et al., 1999; Sturaro, 2003). The use of data sets with variable start times can complicate the comparisons of any resulting time series, however, the following analysis embraces these differences as evidence of the robustness of the analysis method.

The first step is identifying the isentropic layers that house the austral-winter jets. This was done by finding at which isentropic layer the maximum wind speed was observed in each grid column (between 10 and 80°S) at each analysis time in JJA from the JRA-55 dataset. The use of isentropic space here differs from the insightful approach by Manney et al. (2017) and Manney and Hegglin (2018) which employed separate latitude and elevation criteria to differentiate between the STJ and the POLJ. The JRA-55 dataset was chosen for this analysis step because its temporal length and its horizontal and vertical resolutions fall between those of the other two datasets.

Using the General Meteorology Package (GEMPAK) (desJardins et al. 1991) and JRA-55 output from 1958-2019, two scripts were created using the GDCSV program from GEMPAK to

find the maximum wind speeds and the corresponding theta values at those wind speeds (respectively from the script titles). These values were found via the functions:

L<sub>YR</sub>\_M<sub>XMN</sub> (MAG(OBS) & MXVAL | 1000-100)

and

L<sub>YR</sub>\_M<sub>XMN</sub> (MAG(OBS) & MXOUT & THTA | 1000-100)

as the GFUNC in GEMPAK. The files loop through every day for every year at 00 UTC and forecast hour of 00 UTC. The script outputs a CSV file for every single day of the JRA-55 data with the maximum values at all the grid points on that day.

Data points needed next were the maximum wind speed, the  $\theta$  value at that wind speed location, the coordinates, date, and time. A python script was created that loops through the maximum wind speed files to get these outputs. Using set variables, the maximum wind speed and coordinates are copied for each day in a list. The next step loops through all the potential temperature files comparing the latitude and longitude to every location until a match is found. Then the potential temperature at that location is added to the list with the coordinates and wind speed. This is repeated for all the files in the temperature directory. Once completed, a new file is written containing the latitude, longitude, highest wind speed per day, potential temperature at that wind speed, each day of the given data, and time.

Only grid columns that had an integral average wind speed exceeding  $30 \text{ ms}^{-1}$  in the 100-400 hPa layer were considered, following Koch et al. (2006). The results in Figure 2.1a show three maxima in the distribution that are the three jet features found in the following isentropic layers: 305-320, 340-355, 395-410 K. The latter layer is likely the polar night jet as it lies near 400 K which is located above 100 hPa, therefore in the lower stratosphere, and is not a focus of this present analysis. We refined the constraints on the layers based on the Gallego et al. (2005) results

where it is implied that the STJ peaks near 30°S and the POLJ peaks near 50°S. The latitude bins were set to 0-40°S for the STJ and 40-65°S for the POLJ, and further analysis of these constraints showed the isentropic layer for the STJ to be 340-355K and 310-325K for the POLJ (Figure 2.1b). These results are consistent with previous studies, which was expected as similar methods were utilized (Bals-Elsholz et al. 2001, Nakamura and Shimpo 2004, Gallego et al. 2005). It is important to note that of all qualifying columns (to 380K), 53.8% of the columns in the 0-40°S bin (STJ) were in the 340-355K layer while 46.8% of the columns in the 40-65°S bin (POLJ) were in the 310-325K layer supporting the isentropic assignments for the two species mentioned previously. It is abundantly clear that the STJ is the dominant jet feature in the SH winter and is consistent with prior analyses (e.g. Bals-Elsholz et al. 2001, Nakamura and Shimpo 2004, Gallego et al. 2005).

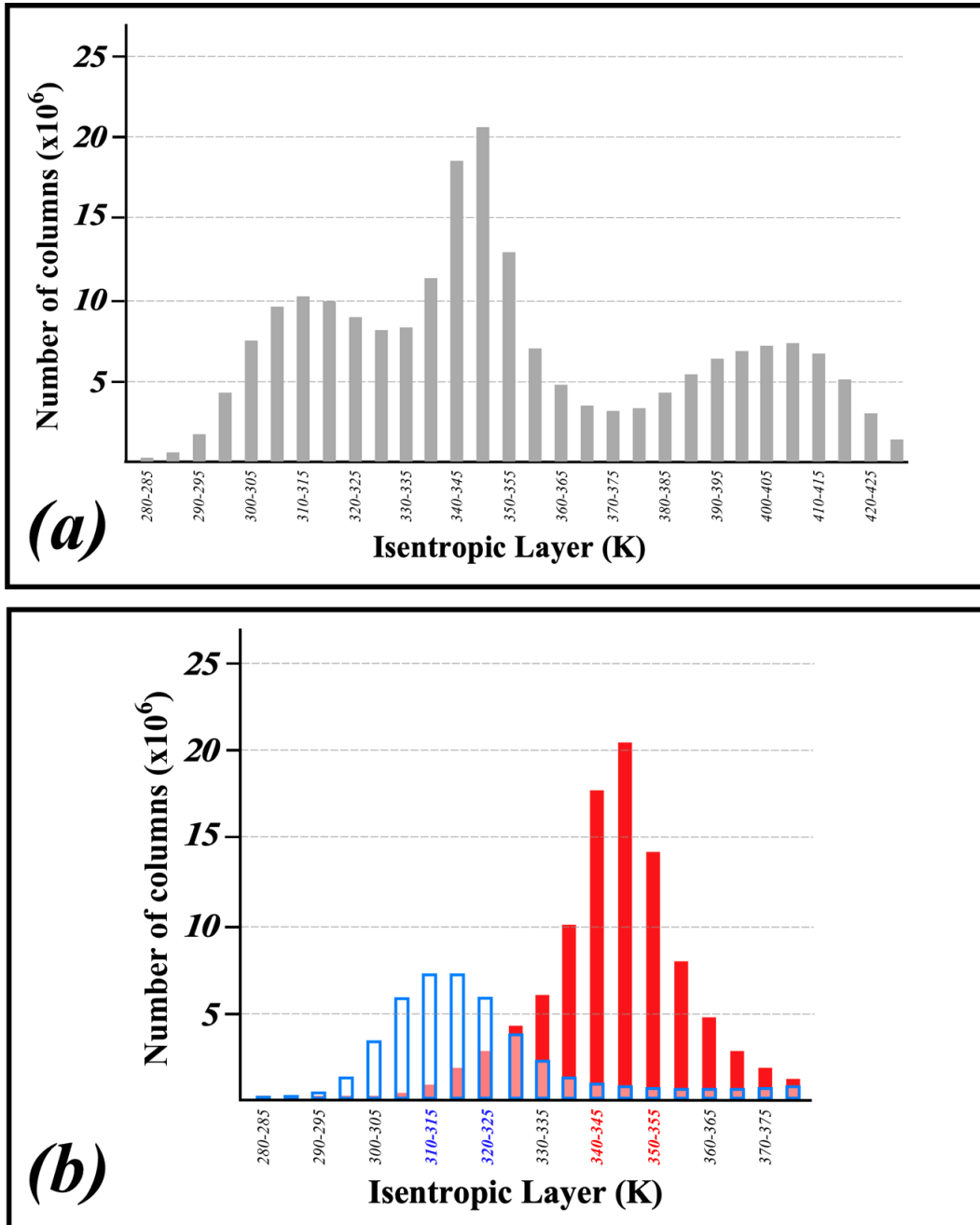


**Figure 2.1** (a) Distribution of grid-column maximum wind speeds found in the isentropic layers from 10-80°S for every 6h analysis time in JJA from 1958-2019 from the JRA-55 reanalysis. (b) As in (a) except limited to (i) grid columns in which the integral average wind speed from 400-100 hPa exceeded 30 ms<sup>-1</sup> and (ii) to latitudes 0-40°S for the STJ (red) and (iii) latitudes 40-60°S for the POLJ (blue).

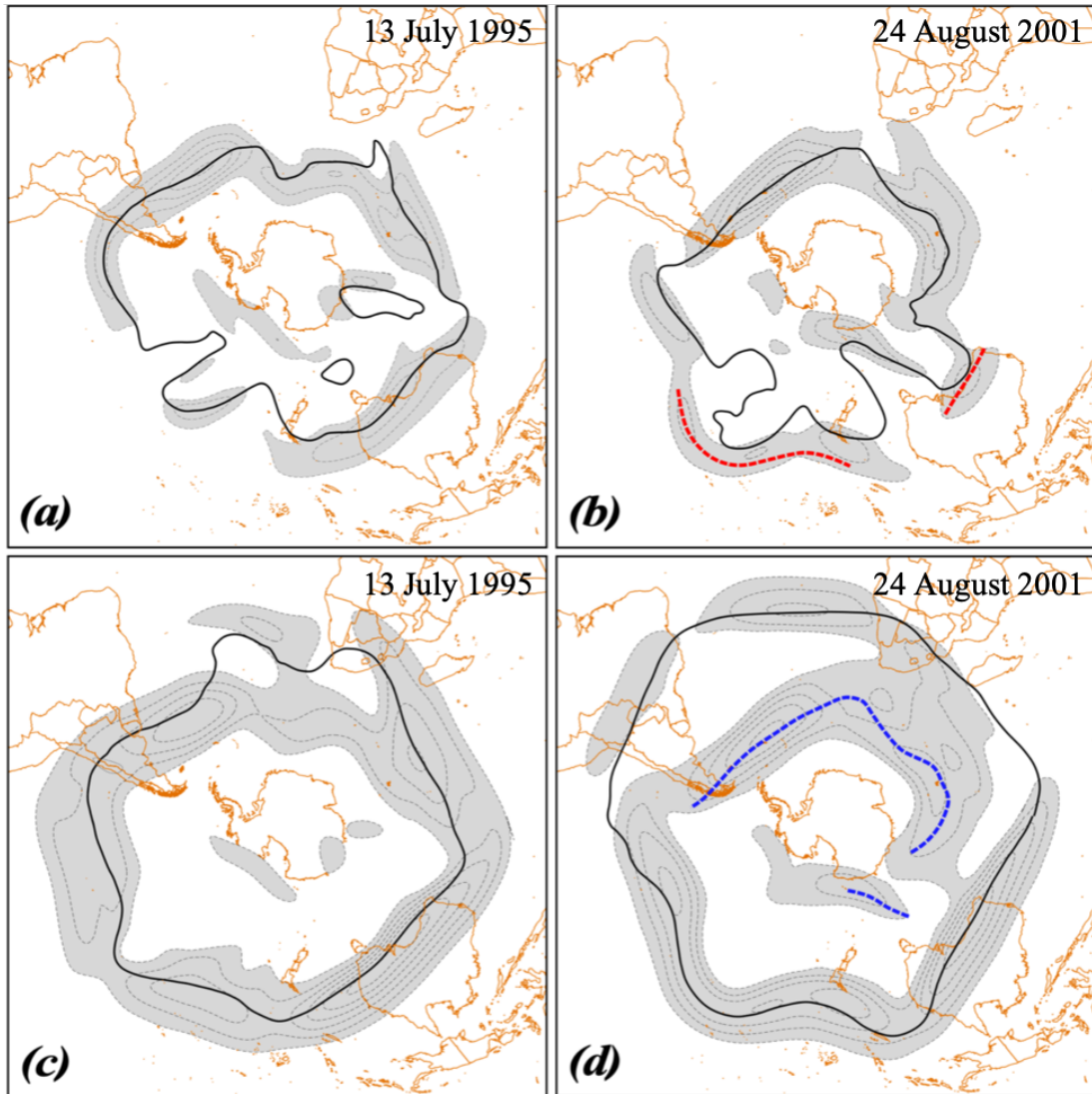
The following analysis method to find the waviness of the jets involves circulation which requires the calculation of contour length. As such, fair comparison among the different datasets requires adoption of a uniform grid spacing. All three datasets were bilinearly interpolated onto isentropic surfaces at 5K intervals (from 280-380K) and 2.5° latitude-longitude grid spacing using programs within the GEMPAK (desJardins et al. 1991). The 2.5° grid spacing was the lowest common resolution between the datasets, so direct comparisons between all three reanalyses could be made. For both jets, the average zonal and meridional wind speeds as well as the average PV were calculated from the four times daily data. Consideration of the QGPV, Equation 1, following Cunningham and Keyser (2004), demonstrates that local maxima in the cross-flow gradient of QGPV are collocated with maxima in the geostrophic wind speed. In the SH, the jets lie on the high PV edge of this PV gradient.

Since jets are always in regions of a strong PV gradient, a proxy for the axis of maximum wind speed (“core”) of a jet is one of several isertels within the strong gradient region. These are defined in this study as a “core isertel” and can vary each day. The goal is to quantify the daily departure of these core isertels from zonality so that we can assess the waviness of each jet. In order to perform this analysis, the circulation equation is considered, given by

$$(3) C = \oint \vec{U} \cdot d\vec{l}$$

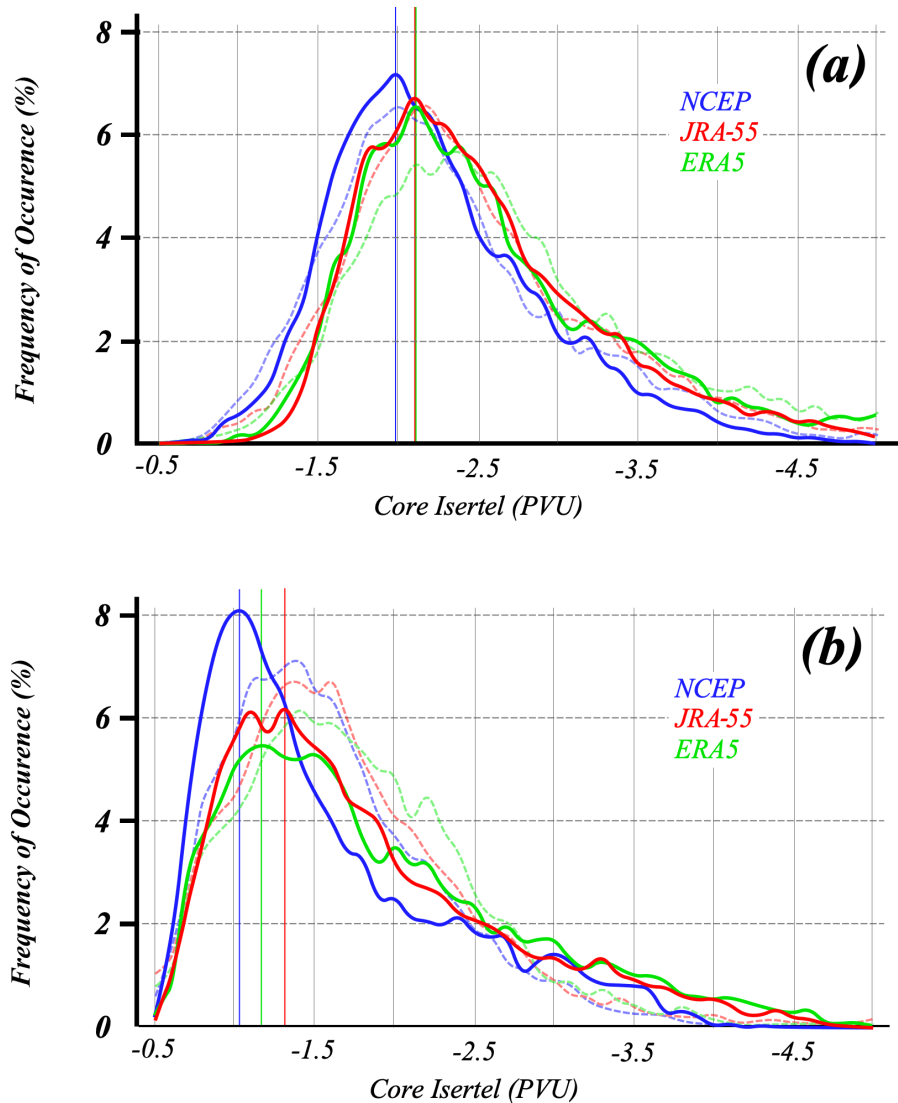
where C along isertels from -0.5 to -5.0 PVU with 0.1 PVU intervals (1 PVU = 10<sup>-6</sup>m<sup>2</sup> K kg<sup>-1</sup> s<sup>-1</sup>) in each jet layer every day. The isertel where the average  $|\vec{U}|$  per unit length is maximized is considered the core isertel as a jet core proxy.

Figure 2.2 displays the objectively identified core isertel (in black) for four randomly selected cases. They lie very near, or at, the center of the analyzed isotach maxima around the hemisphere with physically defensible exceptions. For instance, the red dashed lines in Fig. 2.2b indicate portions of the bold black line in Fig. 2.2d (i.e. the overlying STJ core). The overlap suggests that those portions of the isotach maxima in Fig. 2.2b that are somewhat removed from the POLJ core isertel are the lower portions of the overlying STJ core. Similarly, a region of isotach maxima in Fig. 2.2d has a blue dashed line where in Fig. 2.2b there is a bold black line through the maxima, clearly indicating that this area poleward of the STJ core isertel is part of the underlying POLJ core.



**Figure 2.2** (a) Isotachs of the daily averaged wind speed (contoured every 10 ms<sup>-1</sup> and shaded above 30ms<sup>-1</sup>) and the core isertel (bold black line; -1.3 PVU) in the 310-325K isentropic layer on 13 July 1995 from the JRA-55 reanalysis data. (b) As in (a) but for 24 August 2001 and the core isertel value is -2.0 PVU. Dashed red line indicates portion of the core isertel from the overlying STJ layer (depicted in (d)). (c) As in (a) but for wind speeds and core isertel in the 340-355K isentropic layer on 13 July 1995 (-3.6 PVU). (d) As in (c) but for 24 August 2001 and core isertel value is -1.4 PVU. Dashed blue line indicates a portion of the core isertel from the underlying POLJ layer (depicted in (b)).

This method does not require that the core isertel be the same in both jet layers on a given day nor that it be the same from day-to-day in a given jet layer. Thus, it is important to examine the distribution of the core isertel in each jet layer over the entire time series. Since a constant value of the core isertel is not mandated in this process, it is useful to see the distribution of the daily values of core isertel as a check. Figure 2.3 portrays the frequency of occurrence of the core isertels in both the STJ and POLJ layers for each of the three data sets. The STJ core isertels peak between -1.95 and -2.1 PVU across the three datasets. Considering all three datasets, 81.5% of all JJA days exhibit a core isertel between -1 and -3 PVU in the STJ layer. The POLJ distribution is shifted toward higher PV values. Overall, 74.8% of JJA days had a core isertel between -1 and -3 PVU in the POLJ layer. The SH jets' frequency of occurrence in the isertelic bins match anticipatedly well with the NH jet species from Martin (2021), even when accommodating for the different isentropic layer for the austral POLJ. The frequency of the days that have a core isertel in the range of 1-3 PVU, where one might expect it to be, shows the robustness of the method. Despite the differences in the isentropic layers of the two jets between the hemispheres, the distribution of the daily values of the core isertels are the same.



**Figure 2.3** The frequency of occurrence of the core isertel value for each reanalysis time series in (a) the STJ layer and (b) the POLJ layer. In both (a) and (b), the SH distributions are from NCEP/NCAR (solid blue), JRA-55 (solid red), and ERA5 (solid green) reanalyses. The NH distributions are shown the same but as dashed lines. In (b), the NH distributions are from the 315-330 K layer which is where the POLJ resides in boreal winter. Vertical blue, red, and green lines in (a) and (b) indicate the peak values of the core isertel in each layer from each data set. Isertel values are given in potential vorticity units (PVU,  $1 \text{ PVU} = 10^6 \text{ K m}^2 \text{ kg}^{-1} \text{ s}^{-1}$ ) and multiplied by -1 for the NH values.

The average latitude of the core isertels for both jets from each of the three reanalyses data sets used in this study is shown in Figure 2.4a. The analyses return essentially identical results for the core isertel of the STJ and very nearly identical results for the POLJ. Using the NCEP-NCAR reanalysis of the JJA average 200 hPa isotachs and superimposing them on the STJ core isertels (Figure 2.4b) shows that the average core isertel accurately represents the axis of the average STJ. For the POLJ, the same relationship is strong but with the 700 hPa averaged isotachs (Figure 2.4c).

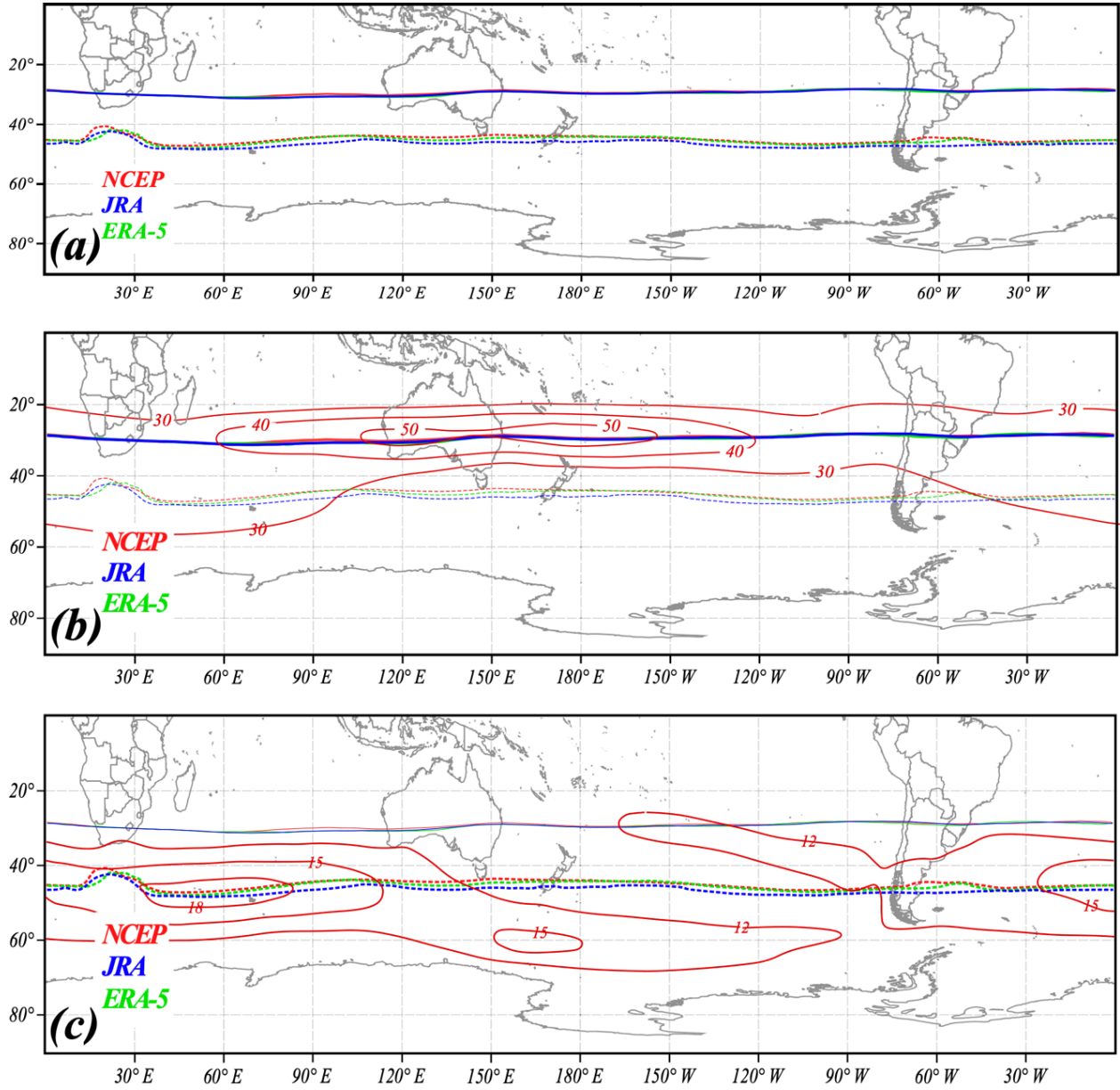


**Figure 2.4** (a) Solid (dashed) lines are the positions of the average core isertels of the STJ (POLJ) from each of the three reanalyses (color coded) used in this study. (b) The thick solid lines are the positions of the average core isertels for the STJ from each of the reanalyses superimposed with JJA average 200 hPa isotachs from the NCEP-NCAR reanalysis. (c) Same as (b) but for the POLJ and 700 hPa isotachs.

The final step in this analysis is to calculate the equivalent latitude, inspired by the method from Huang and Nakamura (2016). The core isertel on any given day within a certain layer encloses a finite area. The equivalent latitude,  $\phi_e$ , is the northern extent of the polar cap whose area is equal to the area (A) enclosed by the core isertel and is given as

$$(4) \phi_e = \arcsin \left[ 1 - \frac{A}{2\pi R_e^2} \right]$$

where  $R_e$  is the radius of the Earth. The meridional departure of the core isertel from its equivalent latitude is measured at each longitude. Where the core isertel crosses the same longitude line more than once, the segment which has larger PV than the one north of the equivalent latitude, or vice versa, is counted. The average latitudinal displacement (ALD) is the sum of all departures divided by the number of longitude lines at the resolution of the data ( $2\pi/2.5^\circ = 144$ ) and is converted into degrees. If the ALD were to be 0.0, that would indicate a perfectly zonal core isertel and the larger the ALD value, the greater the waviness is.

### 3. Results

#### 3.1 Jet Waviness

The waviness of the winter SH jets is shown in Figure 3.1 where it can be seen that the POLJ is wavier than the STJ. The POLJ has become wavier over time from 1958-2019 ( $p < 0.004$ ), increasing by 0.0169 deg/year ( $p < 0.001$ ). The winter SH STJ also steadily became wavier over the same time period ( $p < 0.004$ ), but at a smaller rate of 0.005 deg/year ( $p < 0.001$ ). Within the time series, the waviness of the polar jet appears to have three regimes: 1958-1975, 1976-1998,

and 1999-2019. The changes for the STJ are much less pronounced overall but are still distinct. The following time period trends were the only ones considered in this study. During the most recent time period (1999-2019), trends for both jets are mostly stable but during the previous two periods the trends are of opposing sign. The polar jet decreases by 0.0238 deg/year from 1958-1975 and increases by 0.042 deg/year from 1976-1998. However, the subtropical jet increases by 0.0081 deg/year during 1958-1975 and decreases by 0.0027 deg/year from 1976-1998. None of these trends are statistically significant, but the closest to being significant is the polar jet increasing from 1976-1998 ( $p = 0.02$ ). Further discussion on possible reasoning for these regimes is in section 4.

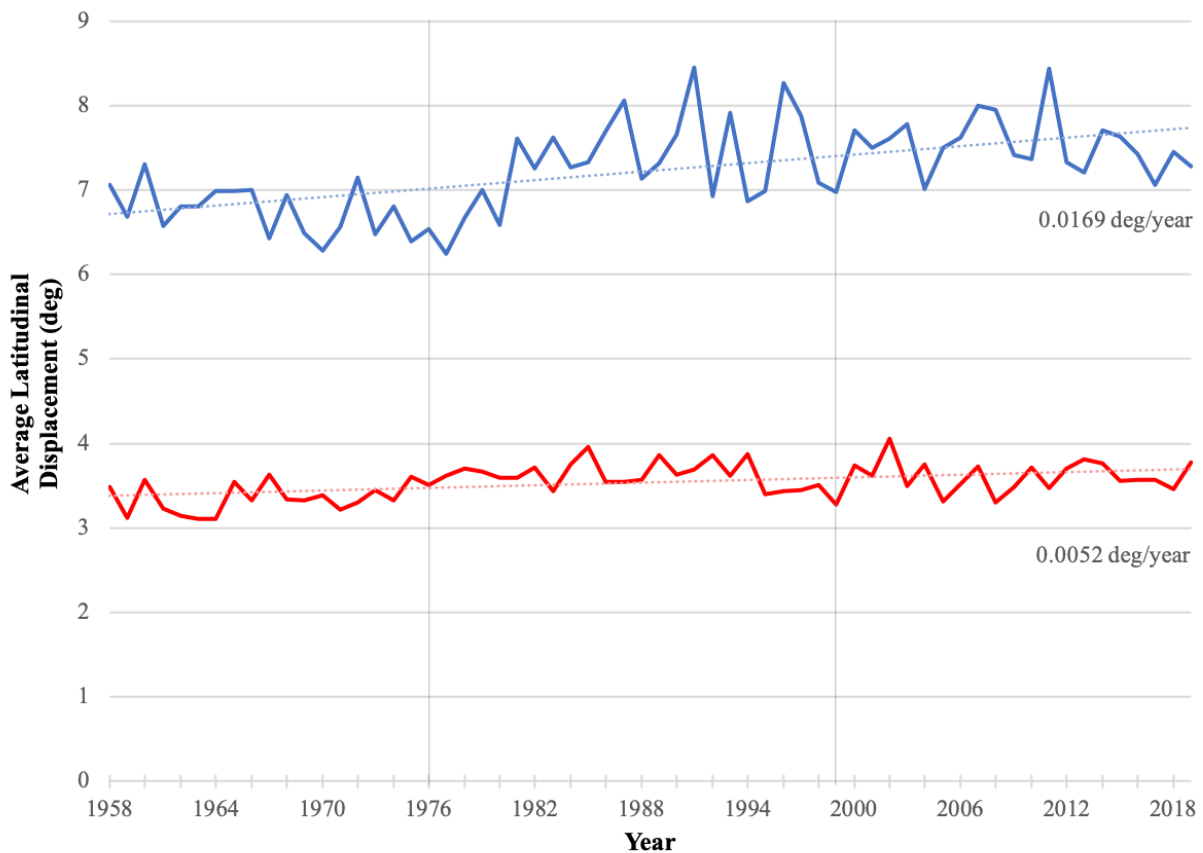


**Figure 3.1** The seasonal average ALD of the STJ (red) and POLJ (blue) for the winter season from the JRA-55 reanalysis. The dotted lines display the trendline for each jet and are significant above the 95% level.

Similarly to the SH, the NH POLJ is wavier than the STJ with both jets systematically becoming wavier over the time series). The SH POLJ is wavier and is trending faster ( $0.017$  versus  $0.009^\circ \text{ yr}^{-1}$ ;  $0.023^\circ \text{ yr}^{-1}$  for NCEP/NCAR since 1958 and  $0.009^\circ \text{ yr}^{-1}$  for ERA5) than its NH counterpart. On the other hand, the STJ in the NH is wavier than the SH STJ but the waviness of both has increased at the same rate of  $0.005 \text{ deg/year}$  ( $0.0125^\circ \text{ yr}^{-1}$  for NCEP/NCAR since 1958 and  $-0.001^\circ \text{ yr}^{-1}$  for ERA5).

The daily ALDs for 1999, a randomly selected year, for the SH STJ and POLJ are shown in Figure 3.2 for each dataset. The low correlation between the waviness of the two species in this example year represents the rule rather than the exception. All told, more than 93 % of the STJ and POLJ ALD seasonal time series constructed for this study are correlated with magnitudes less than 0.3. This strongly suggests the two jets evolve independently with respect to waviness.

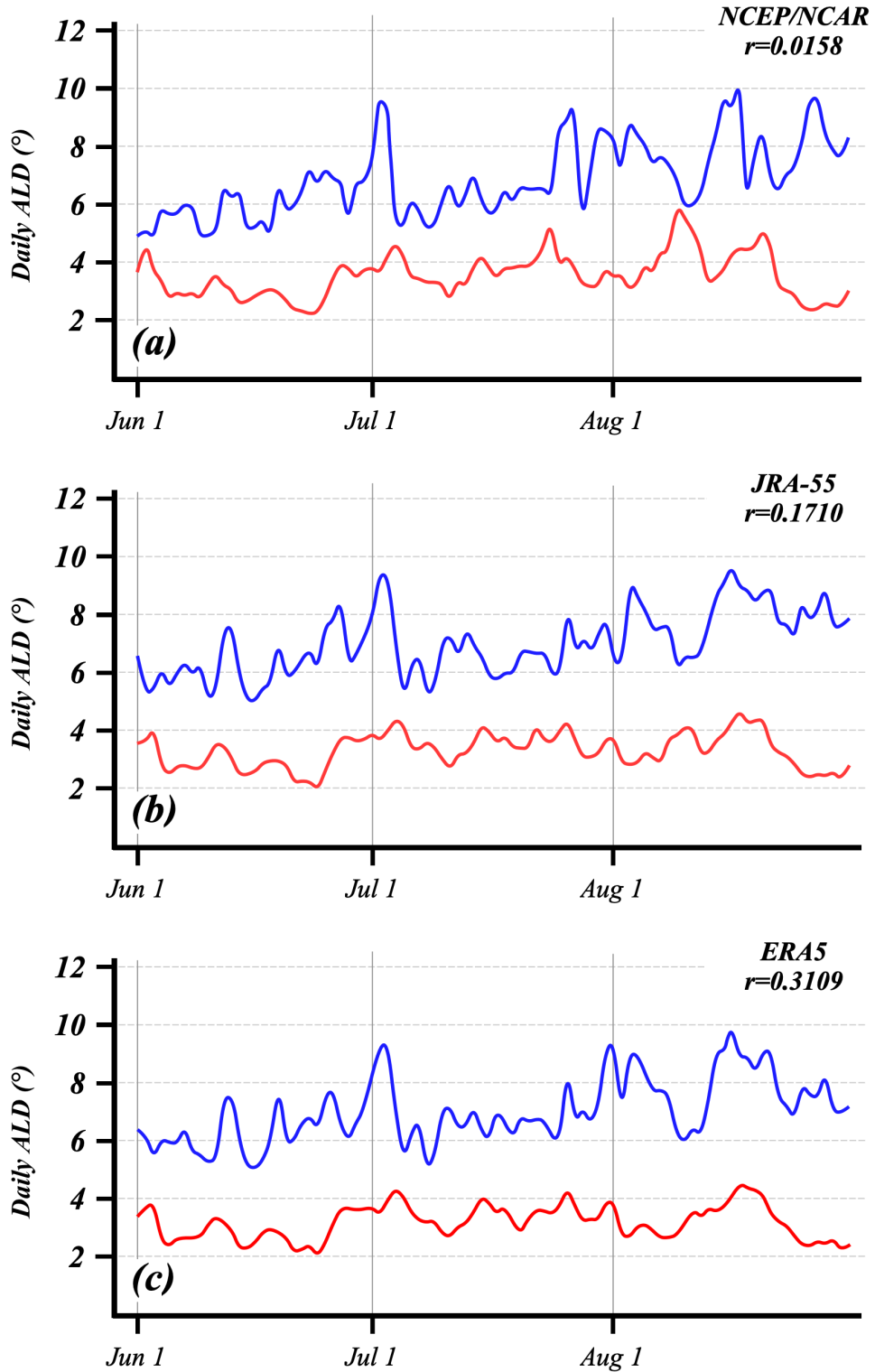


**Figure 3.2** Time series of the daily ALD of the POLJ (blue) and STJ (red) from the (a) NCEP/NCAR reanalysis, (b) JRA-55, and (c) ERA5 dataset for the austral winter in 1999. The correlation between the two time series from each dataset are indicated.

Thus far the analysis has presented elements of the seasonal-average behavior of the austral-winter jets. The methodology allows for evaluation of the daily time series of ALD and such an analysis underlies the presentation in Figure 3.2. Using this daily time series, identifying the waviest and least wavy winter jets since 1958 is accomplished by summing the daily departures from the calendar-day average ALD over the 92 days of each winter season. The overall waviest POLJ averaged over the winter was in 1991 and the least wavy POLJ in winter occurred in 1977 (Figure 3.3). In 2002, the waviest winter STJ occurred while the least wavy STJ was in 1964 (Table 3.1).

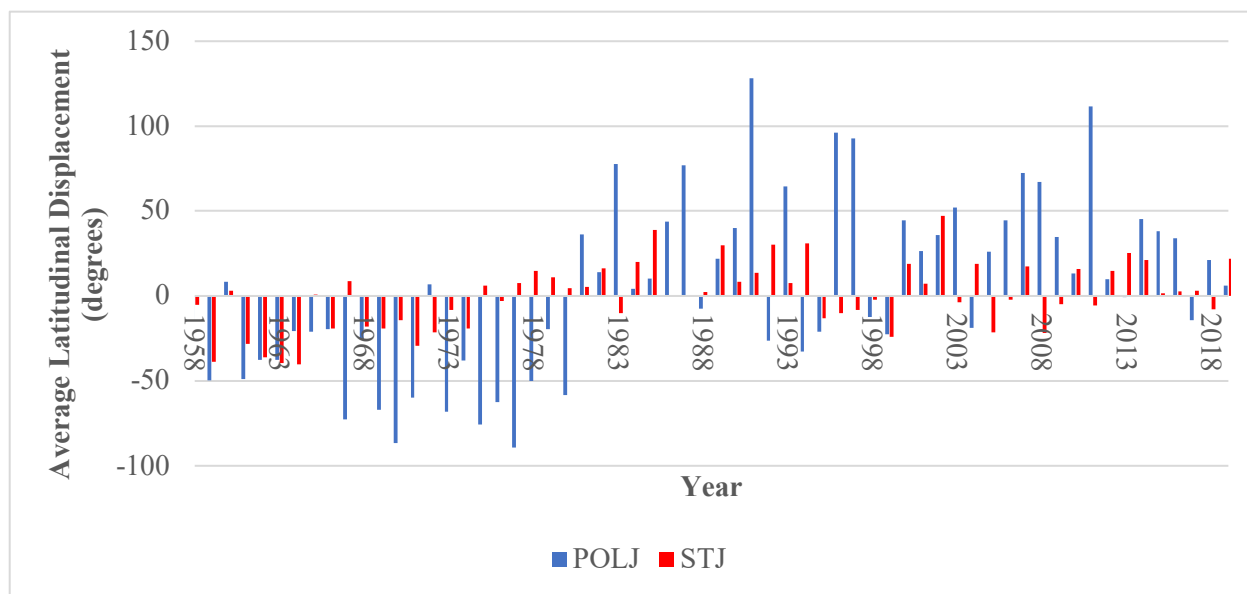


**Figure 3.3** The seasonal waviness values for the POLJ and STJ..

### 3.2 Jet Strength

By definition, the average wind speed along the chosen core isertel on any given day represents the average jet core speed for that species on that day. The SH POLJ speed has

minimally increased over the 62-year period by  $0.0039 \text{ ms}^{-1}/\text{year}$  where the trend is not statistically significant (Figure 3.4). The SH STJ, however, had a greater increase in its speed at a rate of  $0.043 \text{ ms}^{-1}/\text{year}$  which is statistically significant ( $p < 0.001$ ) (Figure 3.4). The STJ is also faster on average at  $48.22 \text{ ms}^{-1}$  while the POLJ averages at  $32.84 \text{ ms}^{-1}$ . The fastest averaged winter jet speed for the POLJ was  $34.84 \text{ ms}^{-1}$  in 1967 and the slowest speed was  $31.09 \text{ ms}^{-1}$  in 1963. A few years later the STJ had its minimum averaged winter jet speed at  $45.14 \text{ ms}^{-1}$  in 1973 while the maximum occurred in 2009 at  $51.21 \text{ ms}^{-1}$ .

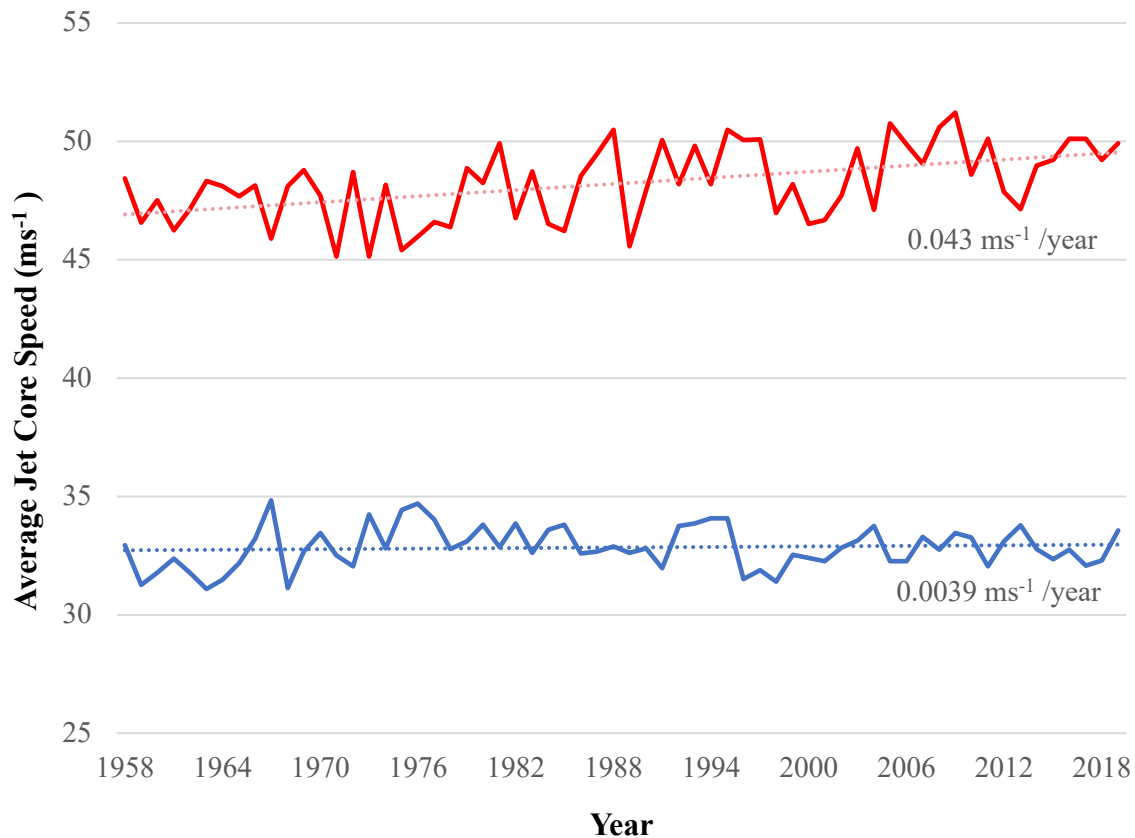


**Figure 3.4** The seasonal average jet core speed along the isertel for the STJ (red) and POLJ (blue) from the JRA-55 reanalysis. The dotted lines are the trend lines for their respective time series.

Comparing the NH results from Martin (2021), the POLJ in both hemispheres show almost no trend in jet core speed and the slight change is not statistically significant. The speeds of these jets differ, though, with the NH POLJ averaging about  $6 \text{ ms}^{-1}$  faster than the SH. For the STJ, the NH jet is much different than the SH as it does not increase (or decrease) in speed over the JRA-55 time series statistically significantly. The SH STJ is overall slightly weaker and also has less interannual variability than the NH STJ (Figure 3.5).

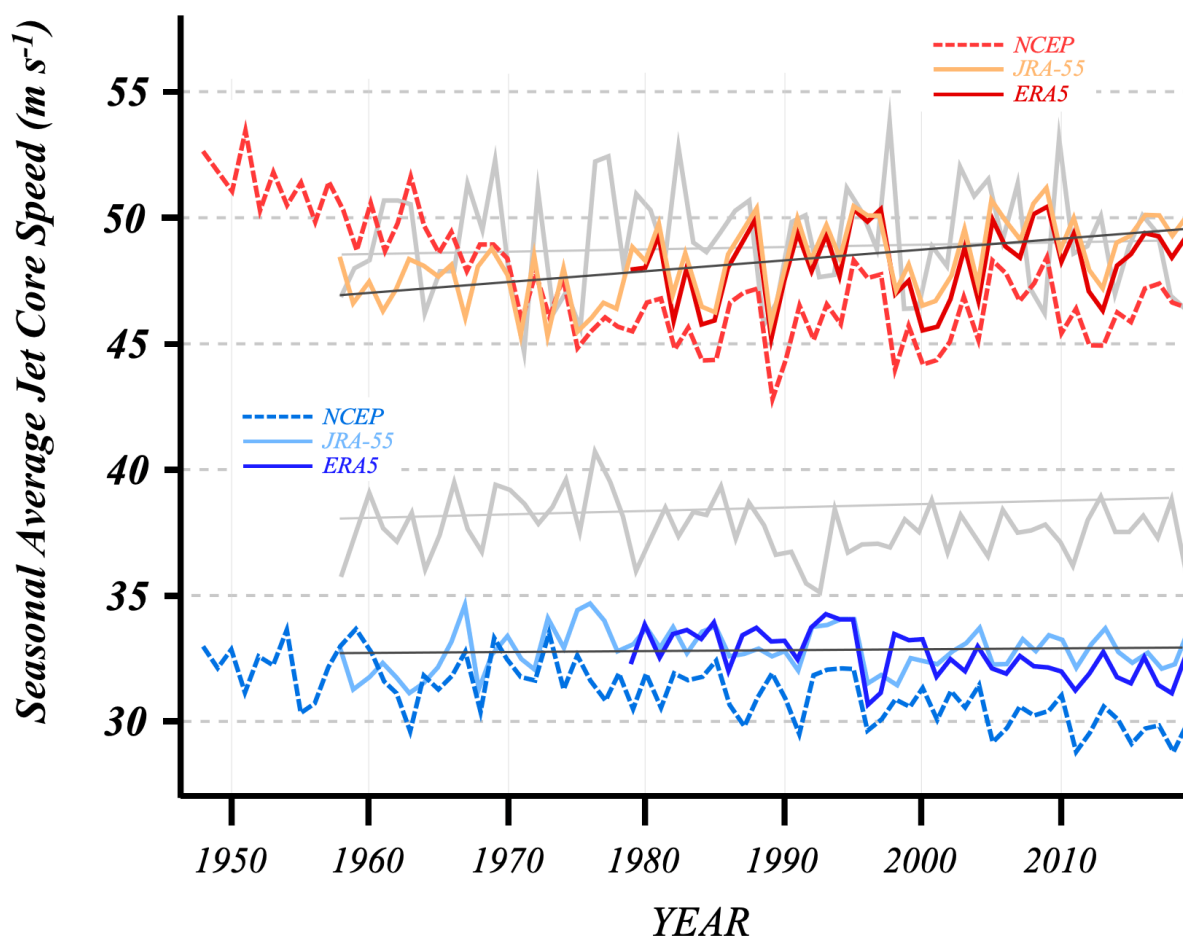


**Figure 3.5** Seasonal-average  $U$  along the core isertel for the subtropical (red lines) and polar (blue lines) jets from each of the three SH reanalysis data sets. The thin black lines are trend lines for each time series from the JRA-55 data. Gray lines are the equivalent boreal-winter  $U$  analysis from Fig. 9 of Martin (2021).

To see how the jet speed changes throughout the season, the daily averaged speeds were considered. The STJ has a somewhat symmetrical curve starting at  $46.59 \text{ ms}^{-1}$  and ending at  $47.06 \text{ ms}^{-1}$  while the middle of the winter season has slightly higher values peaking at  $49.1 \text{ ms}^{-1}$  on July 17<sup>th</sup> (Figure 3.6). For the POLJ, the curve from Figure 3.6 is not symmetrical and drastically drops in speed towards the end of the season. The beginning of winter starts at  $32.93 \text{ ms}^{-1}$ , peaks on July 17<sup>th</sup> at  $34.47 \text{ ms}^{-1}$  and ends at  $27.05 \text{ ms}^{-1}$ .

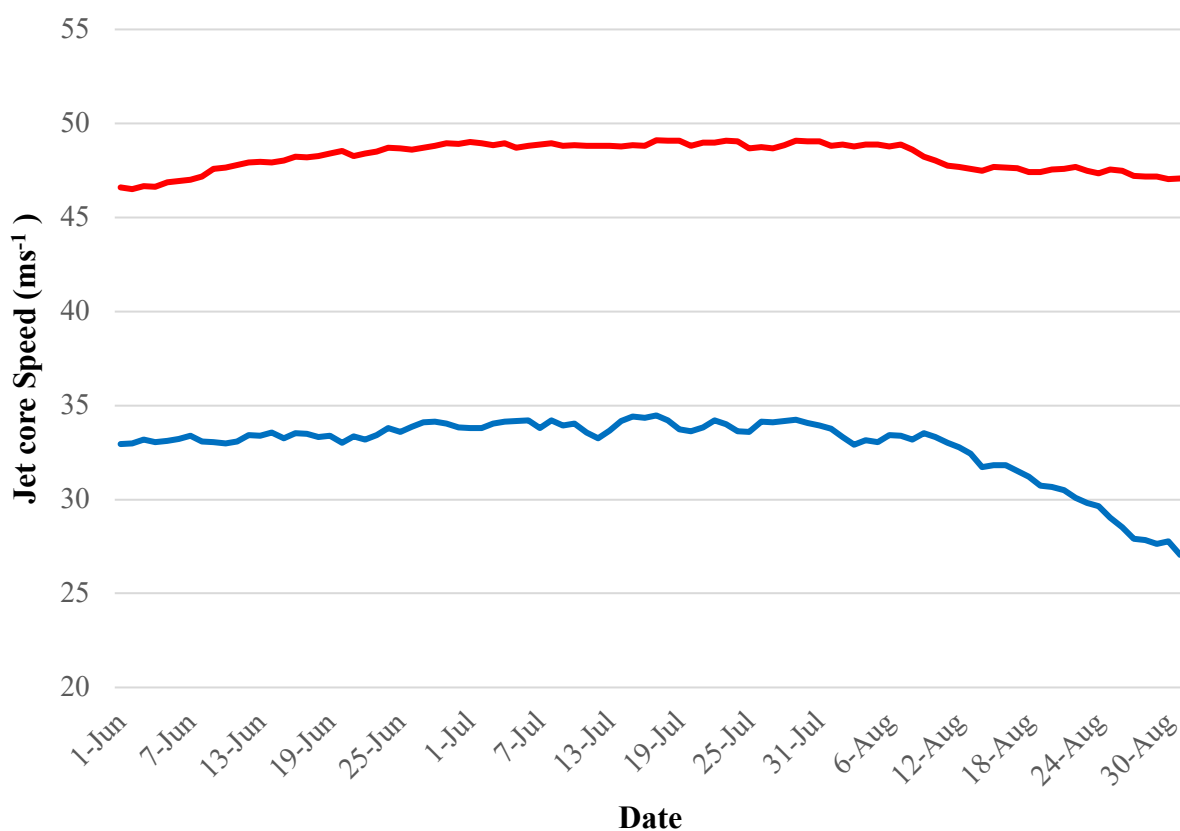


**Figure 3.6** The daily JJA jet core speed averages for the STJ (red) and POLJ (blue).

### 3.3 Jet Equivalent Latitude

Another characteristic of the jets that can be found from the ALD method is the equivalent latitude of the jet, which is a close approximation to zonally averaged position. The POLJ's equivalent latitude has increased, as seen in Figure 3.7, meaning the jet has shifted poleward. The rate at which the POLJ has done so is 0.065 deg/year ( $p < 0.001$ ). The STJ has also shifted towards the pole over this time period but at a rate of 0.022 deg/year ( $p < 0.002$ ) (Figure 3.7). The average POLJ equivalent latitude from 1958-2019 is 44.96°S and for the STJ it is 29.72°S.

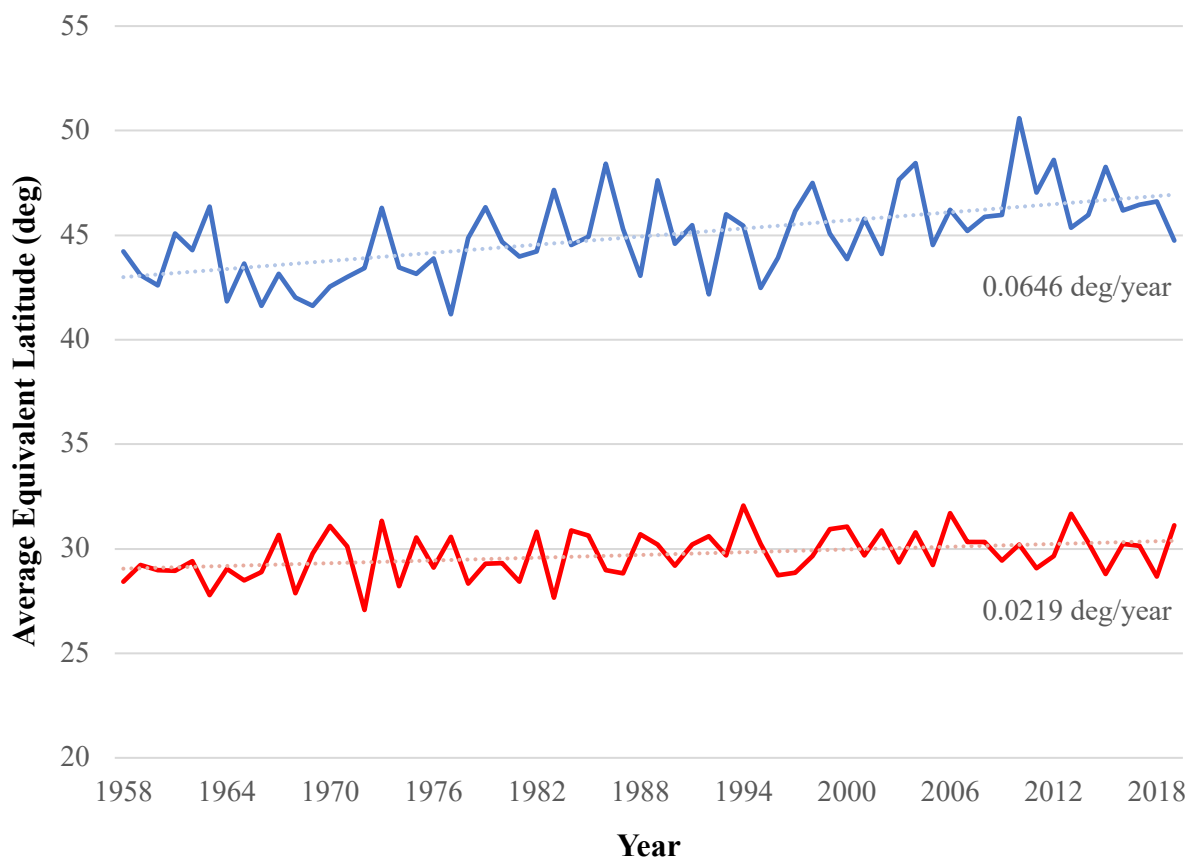


**Figure 3.7** The seasonal average equivalent latitude for the STJ (red) and POLJ (blue) from the JRA-55 reanalysis. The dotted lines are the trend lines for their respective time series.

The poleward shift of the SH POLJ is occurring 3 times faster than the STJ just like in the NH. However, the poleward movement of the SH STJ is statistically significant while such encroachment of the NH STJ is not statistically significant. It is interesting to note that while the SH STJ is located at a latitude roughly similar to the NH STJ throughout the time series, the SH POLJ is  $\sim 4^\circ$  further poleward during winter than the NH POLJ. Overall, a much more systematic and dramatic poleward migration of the two jets has occurred over the last 6 decades in SH winter as compared to NH winter.

The lowest averaged equivalent latitude for the winter season occurred in 1977 at  $41.22^\circ\text{S}$  for the POLJ. In 2010 the POLJ had its maximum averaged equivalent latitude at  $50.59^\circ\text{S}$ . For the STJ the minimum averaged winter equivalent latitude was  $27.07^\circ\text{S}$  in 1972 while the highest was  $32.07^\circ\text{S}$  in 1994.

Throughout the winter season, the equivalent latitude is not constant as seen in the daily averages. The STJ starts the winter at  $28.73^\circ\text{S}$  and slowly increases (shifts poleward) where it then nearly plateaus around mid-June the rest of the season ending at  $30.02^\circ\text{S}$  (Figure 3.8). The POLJ, however, shifts equatorward at a greater range than the STJ moves. The POLJ starts at  $48.86^\circ\text{S}$ , plateaus around late June  $\sim 49^\circ\text{S}$  and then shifts again in mid-August all the way to  $42.44^\circ\text{S}$  (Figure 3.8).

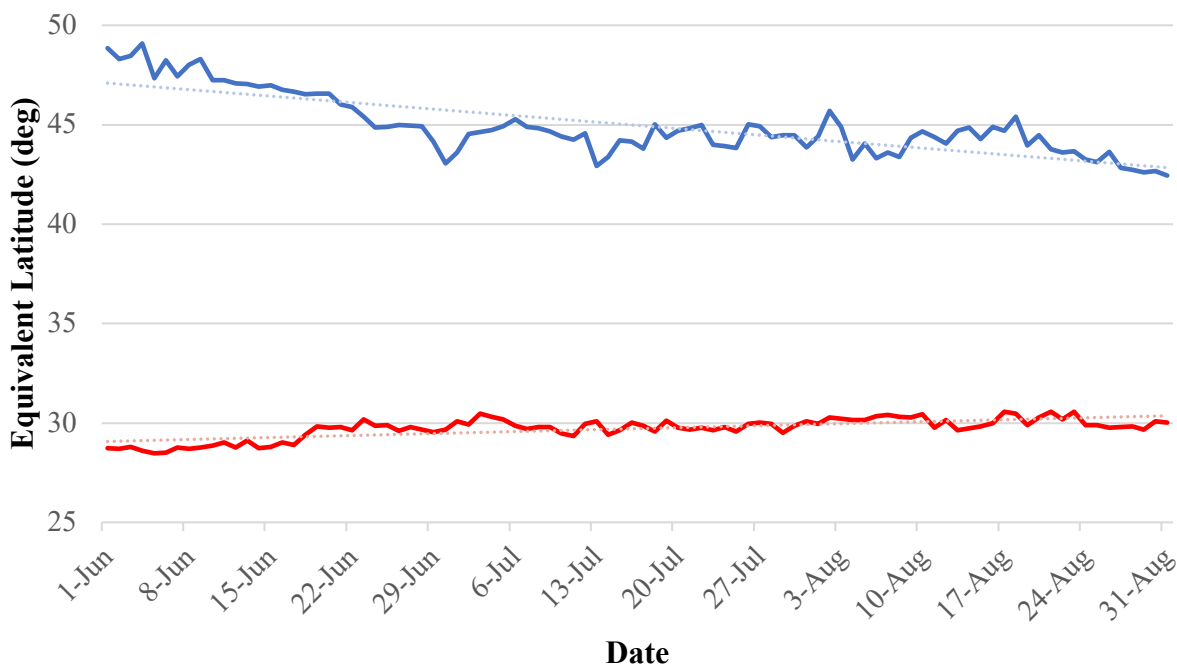


**Figure 3.8** The daily JJA equivalent latitude averages for the STJ (red) and POLJ (blue).

### 3.4 Comparing ALD with SAM

The ALD and waviness of the SH jets may also be related to SAM. Based off of previous studies (Fogt and Marshall, 2020; Gallego et al. 2005), the thought here is an increase in the SAM positive phase would lead to wavier jets. Figure 3.9 shows the histogram of the JJA average SAM index superimposed upon the average JJA ALD of the POLJ from the JRA-55 reanalysis. The index is calculated by projecting the daily 700 hPa geopotential height anomalies poleward of 20°S onto the leading pattern of the Antarctic Oscillation (AAO) of Gong and Wang (1999). The appearance of a positive trend over the time series in SAM seems to be reflected in the increase in ALD. However, the correlation between the two time series is 0.053 suggesting no relationship exists between them, which was surprising.

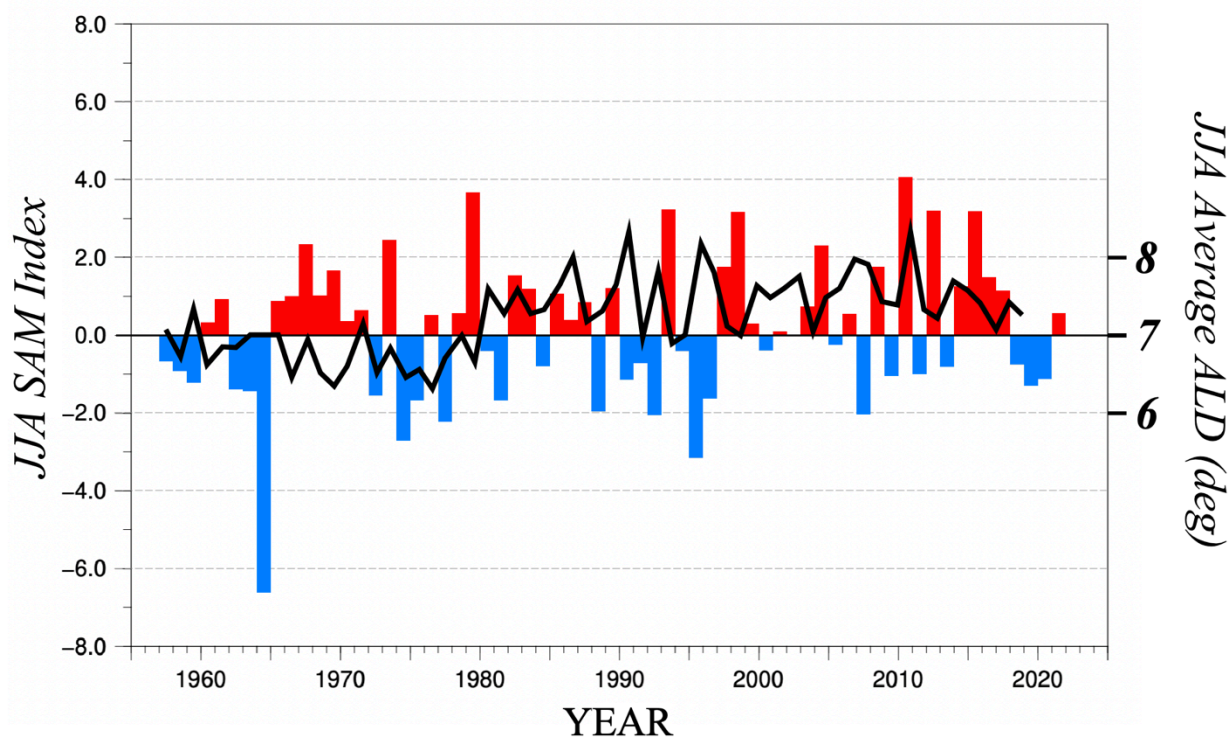


**Figure 3.9** JJA average SAM index as a histogram from NCEP’s Climate Prediction Center and the solid black line is the JJA average ALD of the POLJ from the JRA-55 reanalysis.

Looking further into a possible relationship between SAM and ALD, the extremes in the polarity of the SAM index are considered. The three winter months with the most positive and most negative SAM extremes since 1979 were examined. The core isertels of the POLJ from the JRA-55 reanalysis for each of these months are displayed in Figure 3.10. Positive extremes of SAM (Figure 3.10a, c, e) show a clear poleward movement of the POLJ while negative extremes (Figure 3.10b, d, f) suggest the opposite. There seems to be no systematic connection between the extremes in SAM and the waviness of the POLJ as quantified by ALD ( $R \cong 0$ ), however.

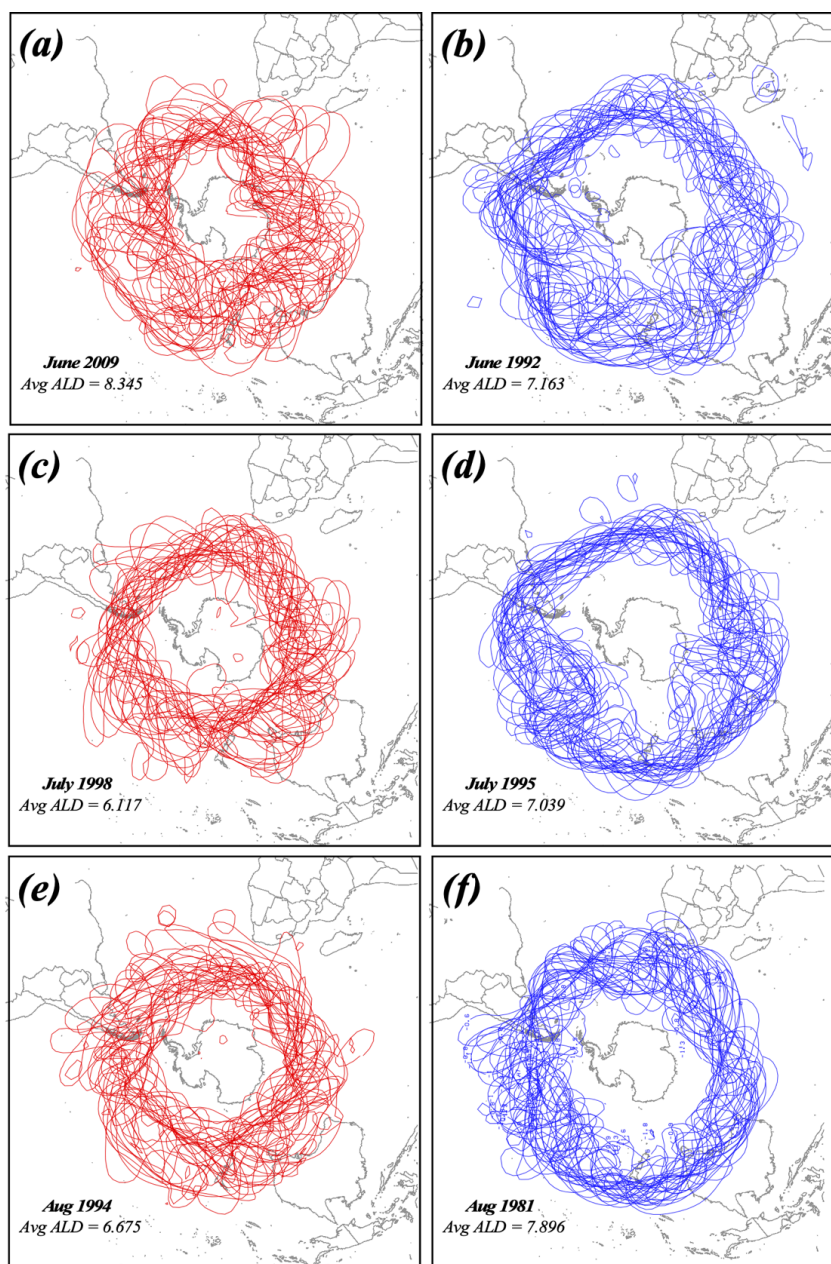


**Figure 3.10** Spaghetti plots of core isertels from SH June, July, and August with maximum positive (red) and negative (blue) SAM indices since 1979. (a) Daily JRA-55 core isertels from June 2009, the June with the most positive SAM in the record. (b) As in (a) but for June 1992, the June with the most negative SAM in the record. (c) As in (a) but for July 1998. (d) As in (b) but for July 1995. (e) As in (a) but for August 1994. (f) As in (b) but for August 1981. Average ALD for the given months are listed in the bottom left of each panel.

### 3.5 Differences in Wavy Seasons

Using the top five most and least wavy winter season jets, composites of the geopotential heights at 500hPa, 250hPa, and 50 hPa were used to create differences between them. Using the 500 hPa height to assess the waviness of the jets is used to show that it in fact is not the best level to get a true sense of the behavior. The 250 hPa height, closer to the tropopause, displays a stronger sense of the jet waviness. At 50 hPa, the difference fields imply that the strength of the polar vortex is influenced by the waviness of both jets. The difference is calculated by subtracting geopotential heights from the least wavy composite from the waviest composite seasons.

The 500hPa composite for the POLJ (Figure 3.11) shows positive height anomalies over the Antarctic continent, Amundsen Sea, and Bellinghausen Sea as well as south of the tip of Africa. Negative anomalous heights are found over the Atlantic Ocean, especially off the west coast of southern Africa, west of southern South America, and near northern New Zealand, suggestive of a negative SAM. With the strongest negative anomaly occurring near the Cape of Good Hope, that may imply a weakening of the zonal winds in that area. The STJ has similar spots but with opposing signs (positive) west of South America and the Bellinghausen Sea along with west and south of Africa, suggestive of a positive SAM. There is a tripole of negative heights over the Amundsen Sea, off the coast of Enderby Land and Wilkes Land.

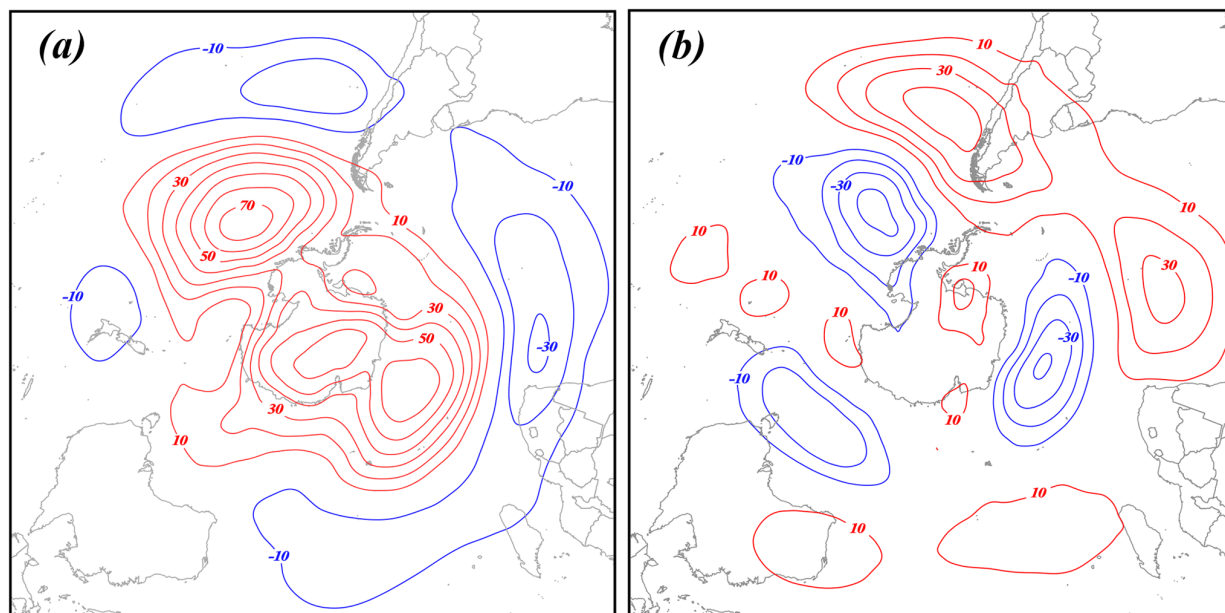


**Figure 3.11** The 500hPa height differences between the composite waviest and least wavy (a) POLJ and (b) STJ seasons constructed from the JRA-55 reanalysis. See Figure 3.3 for identification of the specific years comprising each composite. Positive (negative) height differences are solid red (blue) lines labelled in meters and contoured every 10 m (-10 m) beginning at 10 m (-10 m).

In the 250 hPa composite for the POLJ (Figure 3.12), there is a dipole of positive height anomalies over the Amundsen Sea and off the Enderby Land coast, with higher heights continuing between the two over Antarctica (similar to the 500 hPa composite, but stronger). The negative height anomalies surround this large area of high heights with a neutral area over Australia. The STJ has more positive height anomalies and layout with a tripole of low height anomalies over the Amundsen Sea, south of Tasmania and off the Enderby Land coast (similar to the 500 hPa composite, but stronger). The positive height anomalies both surround and go between the three strong negative anomalies. The strongest positive height differences occur off the eastern coast of

Chile and near the center of the southern Atlantic Ocean. The similar patterns between the 500 and 250 hPa levels suggests equivalent barotropic structure in the troposphere.

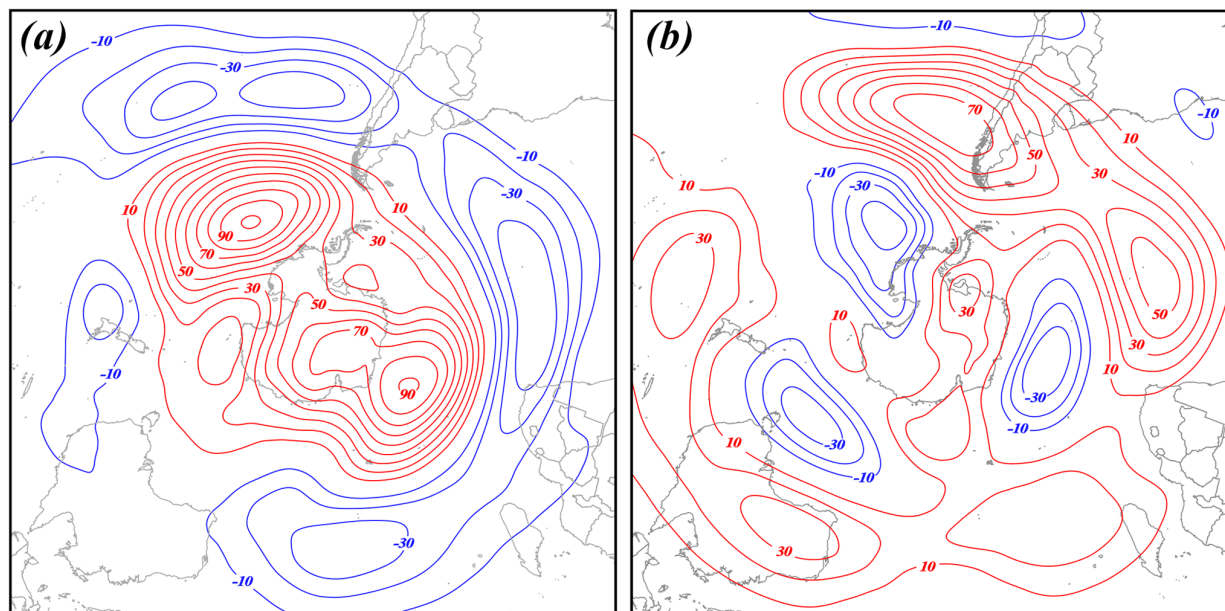


**Figure 3.12** As in Figure 3.10 but for 250 hPa height differences.

For the POLJ, the 50 hPa composite (Figure 13) shows a dipole of positive height anomalies in a very similar pattern to the 250 hPa composite, it is tighter and stronger with the negative heights surrounding closer in. The negative heights reach into the Wilkes and Victoria Land regions with the peak being just off the coast of Wilkes Land and Queen Mary Coast. In the STJ composite, the pattern has drastically changed compared to the lower pressure levels. The positive height anomalies are in a dipole pattern with the strongest areas east of southern Chile and off of Queen Mary Coast. Only a small area of negative height anomalies occurs off the coast of Marie Byrd Land. For the POLJ, the height field suggests an anticyclonic circulation anomaly over East Antarctica, north of the pole, in wavy years. With such a flow, the strength of the vortex could be compromised. Wavy years for the STJ in the height fields imply a diminished and displaced

polar vortex. In both cases, it appears that an unusually wavy POLJ or STJ would have a weakened SH polar vortex compared to normal.

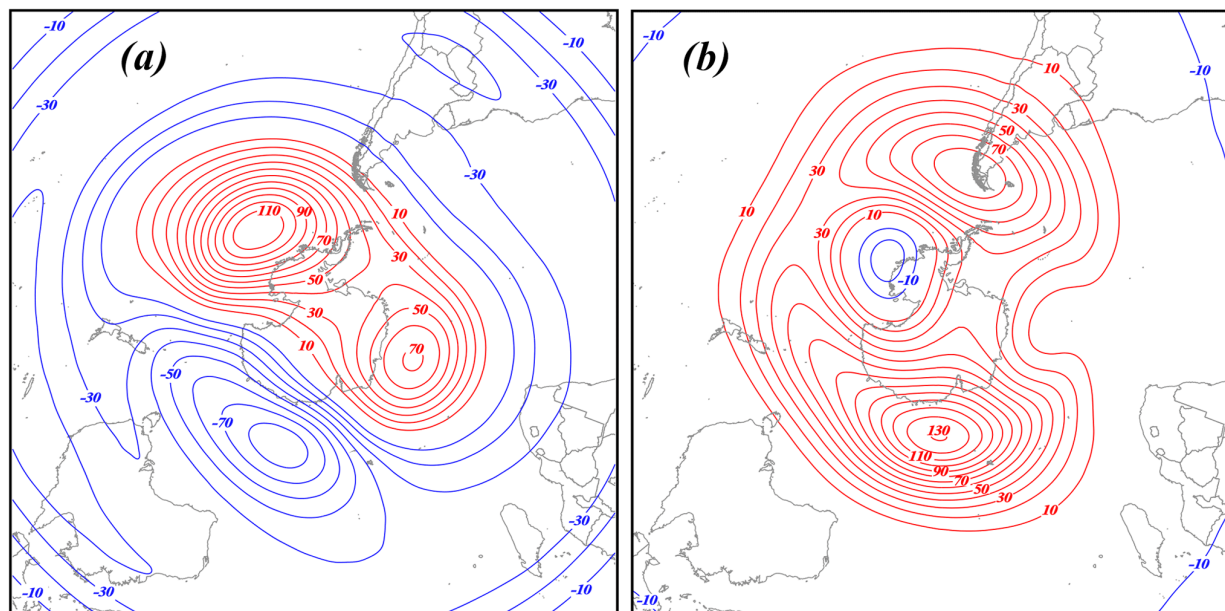


**Figure 3.13** As in Figure 3.10 but for 50 hPa height differences.

#### 4. Discussion

Annual JJA jet strength results are similar to previous studies (Pena-Ortiz et al. 2013, Chenoli et al. 2017) in that the POLJ and STJ are increasing in speed, though minimally for the POLJ. The fact that our results match well with those of previous studies was expected and show similar outcomes for jet strength still occur with different jet identification methods. The poleward shifts of each jet agree with the results of Pena-Ortiz et al. (2013) as well. Maher et al. (2017) had a similarly dynamic definition of the STJ, but they found no evidence of a poleward shift of the SH wintertime STJ. We suggest that the emphasis on empirically identifying a core isertel rather than the maximum gradient of theta on a predetermined isertelic surface (i.e. 2 PVU as the dynamic tropopause), may account for this difference. Since there are no other direct comparisons to finding

the waviness of the SH jets, this project outlines the first results of how the waviness of the jets has changed in recent time. Studies have considered the zonal versus more meridional flow with ZW3 and ZW1, SAM influences on jet behavior as well as ENSO and its effects on the jets. Further discussions on these relationships are below.

#### 4. 1 Connections to Climate Modes

Positive SAM phase is becoming more frequent due to increased greenhouse gases (King et al. 2023, Marshall 2003) and correlates to poleward movement and increased strength of the POLJ. However, the STJ has the same trends, but a positive SAM phase normally has seen equatorward shifts and decreased velocity (Gallego et al 2005). Another difference is that the circumpolar vortex strengthens with positive SAM (Marshall 2003), but the increased waviness of the POLJ does not match with that behavior. During an El Niño phase, the STJ becomes stronger (Gillett et al. 2021), which may have implications on the waviness, or lack thereof, during such a phase.

The synchronization and coupling of climate modes (ENSO, the Pacific Decadal Oscillation, the North Atlantic Oscillation, and the North Pacific Index) provides a marker of a shift in the state of the climate (Swanson and Tsonis 2009). There have been 5 noted times when this synchronization had occurred when the climate system distinctly changed: 1910-20, 1938-45, 1956-60, 1976-81, and 1999-2002 (Swanson and Tsonis 2009). The waviness of both jets appears to have three regimes (1958-1975; 1976-1998; 1999-2019) marked by a change in the latter two time periods, particularly the POLJ. The combination and coupling of multiple climate modes occurring at one time could be the reason for the alignment of the regime changes in the waviness of the SH jets.

## 5. Conclusions

The analysis presented here extends the application of a method developed by Martin (2021) to assess the waviness of the tropopause level subtropical and polar jets in the southern hemisphere. With a warming world, the jets behavior is expected to change and become wavier along with the increase in average temperature. The impacts of wavier jets could lead to stronger storms and impact the weather and climate around the world. The results demonstrate that both of the jets have become systematically wavier over the past 60+ years. Since the two jet species are uncorrelated, both in the NH and the SH, this suggests that the jets do not influence one another throughout the winter. Though there are some similarities, there are distinct and fundamental differences between the two jets between the hemispheres. Both the SH and NH POLJ exhibited no trend in their average speed over the time series, but the SH POLJ is notably slower than in the NH. The STJ in both hemispheres have similar speeds, but the SH STJ has undergone a systematic, statistically significant increase in its core speed since about 1960. There is potential for faster jet streams to increase storm severity (Shaw and Miyawaki 2023). In the SH, both jets have shifted poleward at a statistically significant amount with the POLJ moving about 3 times the rate as the STJ, but in the NH only the POLJ had a statistically significant poleward migration over the time series.

Circulation differences between the waviest and least wavy POLJ and STJ seasons are manifest in both the troposphere and lower stratosphere. The tropospheric signals are not as clear in the SH as they were in the NH, though (Martin 2021). Interestingly, the analysis implies that when either the POLJ or STJ is wavier than normal in a given winter, the lower-stratospheric polar

vortex is negatively impacted. This is surprisingly different from the behavior of the NH polar vortex in the face of extremes in waviness and a segment of future work.

The results presented here for the SH and comparisons of the NH from Martin (2021) show that in both hemispheres, a wavier than normal STJ during the winter serves to weaken the lower stratospheric polar vortex. However, the STJ and POLJ do not appear to influence each other systematically (as suggested above), they can be phased in a way to promote intense interactions. Instances of such interactions can lead to exceptionally strong lower tropospheric cyclogenesis events that can be seen in hemispheric synoptic maps. Future work will include examining whether such jet interaction-induced cyclogenesis events from specific seasons systematically correspond to episodes of polar vortex weakening. Other work could include finding how coupling climate mode interactions affect both of the jet streams and as such, how weather system tracks may be affected.

## 6. References

- Archer, C. L. and Caldeira, K., 2008: Historical trends in the jet streams. *Geophys. Res. Lett.*, **35**, L08803. doi:[10.1029/2008GL033614](https://doi.org/10.1029/2008GL033614).
- Bals-Elsholz, T. M., Atallah, E. H., Bosart, L. F., Wasula, T. A., Cempa, M. J., and Lupo, A. R.: The wintertime Southern Hemisphere split jet: Structure, variability, and evolution, *J. Climate*, 14, 4191–4215, 2001.
- Banerjee, A., Fyfe, J. C., Polvani, L. M., Waugh, D., and Chang, K., 2020: A pause in Southern Hemisphere circulation trends due to the Montreal Protocol. *Nature*, **579**, 544-548. <https://doi.org/10.1038/s41586-020-2120-4>.

- Barnes, E. A., 2013: Revisiting the evidence linking Arctic amplification to extreme weather in midlatitudes, *Geophys. Res. Lett.*, **40**, 4734–4739.
- Chenoli, S.N., Ahmad Mazuki, M., Turner, J. *et al.*, 2017: Historical and projected changes in the Southern Hemisphere Sub-tropical Jet during winter from the CMIP5 models. *Clim Dyn* **48**, 661–681. <https://doi.org/10.1007/s00382-016-3102-y>.
- Christenson, C. E., Martin, J. E., & Handlos, Z. J. (2017). A synoptic climatology of Northern Hemisphere, cold season polar and subtropical jet superposition events. *Journal of Climate*, **30**, 7231– 7246. <https://doi.org/10.1175/jcli-d-16-0565.1>
- Copernicus Climate Change Service (C3S), 2017: ERA5: Fifth generation of ECMWF atmospheric reanalyses of the global climate. Copernicus Climate Change Service Climate Data Store (CDS), <https://cds.climate.copernicus.eu/cdsapp#!/home>.
- Cunningham, P. and Keyser, D., 2004: Dynamics of jet streaks in a stratified quasi-geostrophic atmosphere: Steady-state representations, *Q. J. Roy. Meteor. Soc.*, **130**, 1579–1609.
- Dätwyler, C., Neukom, R., Abram, N. J., Gallant, A, J. E., Grosjean, M., Jacques-Coper, M., Karoly, D. J., and Villalba, R., 2017: Teleconnection stationary, variability and trends of the Southern Annular Mode (SAM) during the last millennium. *Climate Dynamics*, **51**, 2321-2339. <https://doi.org/10.1007/s00382-017-4015-0>
- desJardins, M. L., Brill, K. F., and Schotz, S. S., 1991: GEMPAK 5 Part I – GEMPAK 5 programmer's guide, National Aeronautics and Space Administration, (available from Scientific and Technical Information Division, Goddard Space Flight Center, Greenbelt, MD 20771), GitHub [code], <https://github.com/Unidata/Gempak/releases> (last access: July 2019).

- Francis, J. A. and S. J. Vavrus, 2012: Evidence linking Arctic amplification to extreme weather in midlatitudes. *Geophys. Res. Lett.*, **39**, L06801, doi:10.1029/2012GL051000.
- Fogt, R. L., and Marshall G. J., 2020: The southern Annular Mode: Variability, trends and climate impacts across the Southern Hemisphere. *WIREs Climate Change*, **11**, 1-24. <https://doi.org/10.1002/wcc.652>
- Gallego, D., P. Ribera, R. Garcia-Herrera, E. Hernandez, and L. Gimeno, 2005: A new look for the Southern Hemisphere jet stream. *Climate Dyn.*, **24**, 607-621. <https://doi.org/10.1007/s00382-005-0006-7>.
- Gillett, Z. E., Hendon, H. H., Arblaster, J. M., and Lim, E.-P., 2021: Tropical and Extratropical Influences on the Variability of the Southern Hemisphere Wintertime Subtropical Jet. *Journal of Climate*, **34**, 4009-4022, <https://doi.org/10.1175/JCLI-D-20-0460.1>.
- Gong, D. and Wang, S., 1999: Definition of Antarctic oscillation index, *Geophys. Res. Lett.*, **26**, 459–462.
- Huang, C. S. Y., & Nakamura, N. (2016). Local finite-amplitude wave activity as a diagnostic of anomalous weather events. *Journal of the Atmospheric Sciences*, **73**, 211–229. <https://doi.org/10.1175/jas-d-15-0194.1>
- Kalnay, E., Kanamitsu, M., Kistler, R., Collins, W., Deaven, D., Gandin, L., Iredell, M., Saha, S., White, G., Woollen, J., Zhu, Y., Chelliah, M., Ebisuzaki, W., Higgins, W., Janowiak, J., Mo, K. C., Ropelewski, C., Wang, J., Leetmaa, A., Reynolds, R., Jenne, R., and Joseph, D., 1996: The NCEP/NCAR 40-year reanalysis project, *B. Am. Meteorol. Soc.*, **77**, 437–470.

- King, J., Anchukaitis, K. J., Allen, K., Vance, T., and Hessler, A., 2023: Trends and variability in the Southern Annular Mode over the Common Era. *Nature Communications*, **14**, <https://doi.org/10.1038/s41467-023-37643-1>
- Kobayashi, S. Y., Ota, Y. Harada, A. Ebita, M. Moriya, H. Onoda, K., et al. 2015: The JRA-55 reanalysis. General specifications and basic characteristics. *Journal of the Meteorological Society of Japan*, **93**, 5–48. <https://doi.org/10.2151/jmsj.2015-001>
- Koch, P., Wernli, H., & Davies, H. C. (2006). An event-based jet-stream climatology and typology. *International Journal of Climatology*, **26**, 283–301. <https://doi.org/10.1002/joc.1255>
- Lewis, J. M., 2003: Ooishi's Observation. *Bulletin of the American Meteorological Society*, **84**, 357-370, <https://doi.org/10.1175/BAMS-84-3-357>.
- Maher, P., Kelleher, M. E., Sansom, P. G., and Methven, J., 2020: Is the subtropical jet shifting poleward?, *Clim. Dynam.*, **54**, 1741–1759.
- Manney, G. L. and Hegglin, M. I., 2018: Seasonal and regional variations of long-term changes in upper-tropospheric jets from reanalyses, *J. Climate*, **31**, 423–448.
- Manney, G. L., Hegglin, M. I., Lawrence, Z. D., Wargan, K., Millán, L. F., Schwartz, M. J., Santee, M. L., Lambert, A., Pawson, S., Knosp, B. W., Fuller, R. A., and Daffer, W. H., 2017: Reanalysis comparisons of upper tropospheric–lower stratospheric jets and multiple tropopauses, *Atmos. Chem. Phys.*, **17**, 11541–11566, <https://doi.org/10.5194/acp-17-11541-2017>.
- Marshall G. J., 2003: Trends in the Southern Annular Mode from Observations and Reanalyses. *Journal of Climate*, **16**, 4134-4143. [https://doi.org/10.1175/1520-0442\(2003\)016<4134:TITSAM>2.0.CO;2](https://doi.org/10.1175/1520-0442(2003)016<4134:TITSAM>2.0.CO;2)

- Martin, J. E. 2021: Recent Trends in the Waviness of the Northern Hemisphere Wintertime Polar and Subtropical Jets. *Journal of Geophysical Research: Atmospheres*, **126**, <https://doi.org/10.1029/2020JD033668>
- Nakamura, H. and Shimpo, A.: Seasonal variations in the Southern Hemisphere storm tracks and jet streams as revealed in a reanalysis data set, *J. Climate*, **17**, 1828–1844, 2004.
- Pena-Ortiz, C., Gallego, D., Ribera, P., Ordonez, P., and Del Carmen Alvarez-Castro, M., 2013: Observed trends in the global jet stream characteristics during the second half of the 20th century. *Journal of Geophysical Research: Atmospheres*, **118**, 2702-2713, <https://doi.org/10.1002/jgrd.50305>.
- Raphael M. N., 2004: A Zonal Wave 3 Index for the Southern Hemisphere. *Geophysical Research Letters*, **31**, L23212, <https://doi.org/10.1029/2004GL020365>
- Shaw and Miyawaki, 2023: Fast upper-level jet stream winds get faster under climate change, *Nature Climate Change*, <https://news.uchicago.edu/story/jet-stream-will-get-faster-climate-change-continues-study-finds>
- Spensberger, C., Reeder, M. J., Spengler, T., and Patterson, M., 2020: The connection between the Southern Annular Mode and a feature-based perspective on Southern Hemisphere midlatitude winter variability, *J. Climate*, **33**, 115–129.
- Swanson, K. L. and Tsonis, A. A., 2009: Has the climate recently shifted?, *Geophys. Res. Lett.*, **36**, L06711, <https://doi.org/10.1029/2008GL037022>
- WMO, 2022: Executive summary. Scientific assessment of ozone depletion: 2022, GAW report, no. 278, Geneva, Switzerland: WMO, <https://library.wmo.int/viewer/42105/?offset=3#page=1&viewer=picture&o=bookmark&n=0&q=> (last access: June 2023).